This is a preprint draft. The published article can be found at: https://doi.org/10.1016/j.compstruct.2022.115651

Please cite this paper as:
Saleh E, Tarawneh, A., Naser M.Z., (2022). "Failure mode classification and deformability evaluation for concrete beams reinforced with FRP bars." *Composite Structures*. https://doi.org/10.1016/j.compstruct.2022.115651

Failure mode classification and deformability evaluation for concrete beams reinforced with FRP bars

Eman Saleh[1,*], Ahmad N. Tarawneh[2], and M.Z. Naser[3]

[1,*] Assistant Professor, Civil Engineering Department, Faculty of Engineering, The Hashemite University, P.O. box 330127, Zarqa 13133, Jordan; Email: emanf_yo@hu.edu.jo

[2] Assistant Professor, Civil Engineering Department, Faculty of Engineering, The Hashemite University, P.O. box 330127, Zarqa 13133, Jordan; Email: ahmadn@hu.edu.jo

[3] Assistant Professor, School of Civil & Environmental Engineering and Earth Sciences (SCEEES), Clemson University, Clemson, SC 29634, USA

[3] AI Research Institute for Science and Engineering (AIRISE), Clemson University, Clemson, SC 29634, USA

E-mail: mznaser@clemson.edu, Website: www.mznaser.com

(*) Indicates the corresponding author.

Abstract

The flexural failure mode of fiber-reinforced polymers (FRP) reinforced concrete (FRP-RC) beams is a key concern in the design and capacity evaluation. Therefore, developing a robust method to identify the failure mode of FRP-RC beams is warranted. This paper presents a support vector machine (SVM) algorithm, together with comprehensive compiled experimental databases and a verified analytical model, to identify and classify the failure mode of FRP-RC beams. The SVM analysis yields "data-driven classification rules" that not only achieved superior performance over ACI 440 guidelines but are also valid for a large range of design parameters. The proposed classification rules are a function of the balanced reinforcement ratio (ρ_{fb}) and height to depth ratio (h/b) of FRP-RC beams. In addition, the verified classification rules recommend increasing the transition zone defined by ACI 440 from $1.4\rho_{fb}$ to $1.55\rho_{fb}$. The study also utilized the verified analytical model to conduct a comprehensive deformability evaluation of FRP-RC members for different failure modes. The results indicate that FRP-RC beams will have sufficient deformability before failure regardless of the failure mode. In addition, to ensure minimum deformability requirements for FRP-RC beams, a limit should be specified on the modulus of elasticity -to-the ultimate tensile strength of FRP ratio. Based on the analysis, a proposed limit of 200 is recommended.

Keywords: Fiber-reinforced polymers, Machine learning, Classification, Failure type, Deformability

1. Introduction

This is a preprint draft. The published article can be found at: https://doi.org/10.1016/j.compstruct.2022.115651

Please cite this paper as:
Saleh E, Tarawneh, A., Naser M.Z., (2022). "Failure mode classification and deformability evaluation for concrete beams reinforced with FRP bars." *Composite Structures*. https://doi.org/10.1016/j.compstruct.2022.115651

Reinforced concrete (RC) structural elements in harsh corrosive environments, such as coastal construction, suffer from deterioration and concrete spalling due to the imposed stresses by the expanded corroded steel bars [1-3]. In addition, corrosion causes loss in steel reinforcing bars cross-sectional area which adversely affect the safety of RC members. The cost of replacing or repairing deteriorated RC elements can be considerably high or impractical, thereby requiring demolition. Consequently, fiber-reinforced polymer (FRP) bars have emerged as a promising alternative to conventional steel reinforcing bars for their advantageous properties, primarily relating to corrosion resistance.

Following the origins of the research conducted in the 1990s, extensive experimental and analytical research works have been conducted to investigate the flexural behavior of FRP-reinforced concrete beams [4-7]. Based on these experimental studies, two possible failure modes for FRP reinforced concrete (FRP-RC) beams have been identified: concrete crushing and FRP bars rupture [8], and associate analytical expressions were formulated to approximate their flexural capacity based on these likely modes of failure. ACI 440.1R-15 design guideline [7] uses the ratio of FRP reinforcement to a balanced reinforcement ratio value (ρ_f/ρ_b) parameter and thresholds of (1.0) and (1.4) to predict whether FRP bar rupture or concrete crushing will occur. When ρ_f/ρ_b exceeds the balanced reinforcement ratio (i.e., $\rho_f/\rho_b \geq 1.4$), concrete crushing is the predicted failure mode while when $\rho_f/\rho_b \leq 1.0$, FRP rupture is the predicted failure mode. For beams with $1.0 \leq \rho_f/\rho_b \leq 1.4$, observations from a large number of studies [8,10-28] indicated that many beams in this range have experienced either concrete crushing or FRP rupture mode of failure; thus, to be compatible with experimental results and to ensure a safe design, the Japanese guideline, the ACI 440 guideline, and other researchers [9-29] suggested classifying these beams to be located in a transition zone that should be designed based on concrete crushing limit state and with a strength reduction factors ϕ linearly interpolated between FRP rupture and concrete crushing ϕ factors (see **Fig. 1**). ACI 440.1R-15 justifies the lower ϕ factor for the transition zone by the fact that a member in the transition zone is controlled by the concrete crushing limit state, however, the member may not fail accordingly. The margin width of the transition region was selected based on a limited number of observations of beams that failed in FRP rupture with $\rho_f/\rho_b \geq 1$ [8, 27,28]. However, different assessment studies of FRP-RC beams databases indicated that beams with ρ_f/ρ_b greater than 1.4 failed by FRP rupture [8]. Therefore, classifying the mode of failure based on ρ_f/ρ_b value of 1 and 1.4 only may not be robust enough and calls for a better classifier.

This is a preprint draft. The published article can be found at: https://doi.org/10.1016/j.compstruct.2022.115651

Please cite this paper as:
Saleh E, Tarawneh, A., Naser M.Z., (2022). "Failure mode classification and deformability evaluation for concrete beams reinforced with FRP bars." *Composite Structures*. https://doi.org/10.1016/j.compstruct.2022.115651

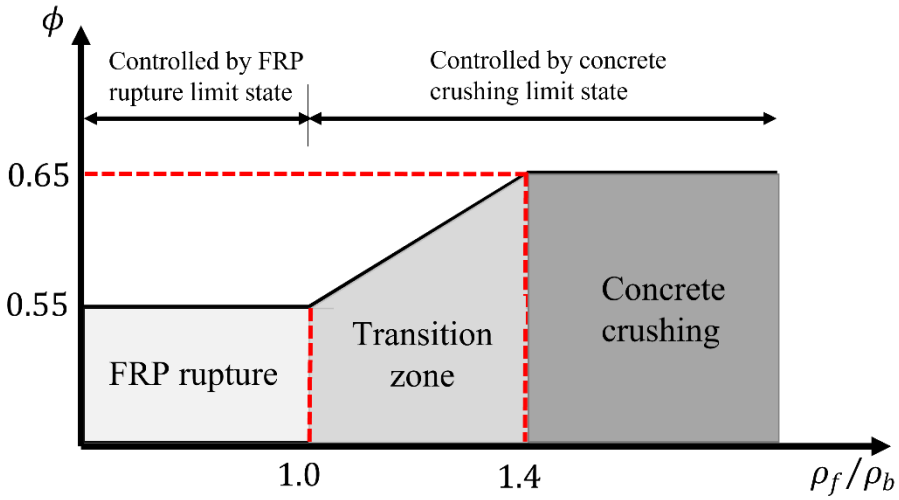

Fig. 1. Flexural strength reduction factor for FRP-reinforced members according to ACI 440.1R-1

In this study, the objective is to formulate a data-driven classifier to predict the likely failure mode of FRP-RC beams by utilizing machine learning (ML) methods. ML has been successfully used in various sectors of civil engineering. Examples of such applications involve load capacity prediction and mode of failure classification of beam-column joints [30], FRP-strengthened reinforced concrete members [31], FRP retrofitted slabs subjected to blast loading [32], masonry shear wall [33], and reinforced concrete columns [34-37]; prediction of the interfacial bond strength between concrete and FRPs [38]; risk assessment [39,40]; damage detection and classification [41,42,43]; prediction of plastic hinge length of reinforced concrete columns [44]. These studies demonstrated that ML is a valuable tool that can outperform existing empirical and numerical methods to solve many complex problems in civil engineering. Nevertheless, to the authors' knowledge, none of the available literature that utilized ML have solved a classification problem in a similar manner to the one explored herein in which the available data only provide two class labels (Class 1: the beam failed in concrete crushing failure mode; Class 2: the beam failed due to FRP rupture); however, the beams that result in any possibility (or class probability) of concrete crushing and FRP rupture that are greater than zero (i.e., class probability > 0 for both classes; both classes are possible) should be classified to belong to a transition zone; thus, the dataset has only two classes that need to be classified into three.

To solve this classification problem, the study employs a comprehensive and up-to-date database of 164 experimental tests of FRP-RC beams and uses 8 input variables that may affect the beam response. To overcome the limited number of tested FRP-RC beams necessary for the classification study, an analytical model based on section analysis (i.e., moment-curvature analysis), is introduced. The objective of the model is to predict the ultimate load and the mode of failure of the FRP-RC beam. Once the analytical model is verified with available experimental

This is a preprint draft. The published article can be found at: https://doi.org/10.1016/j.compstruct.2022.115651

Please cite this paper as:
Saleh E, Tarawneh, A., Naser M.Z., (2022). "Failure mode classification and deformability evaluation for concrete beams reinforced with FRP bars." *Composite Structures*. https://doi.org/10.1016/j.compstruct.2022.115651

results, a large parametric campaign of FRP-RC beams having different combinations of specified properties is designed. The simulated beams combined with actual data of tested FRP-RC beams will be used in the classification study. Support Vector Machines (SVM) with a soft margin is employed for classifying the FRP-RC failure modes using features related to material and geometric properties. The SVM with a soft margin classifier was selected because it provides a clear margin between classes that can be considered as the transition zone. This study also aims to shed more light on this transition zone range and to propose a margin width of the transition zone based on the beam properties or features (e.g., geometric dimension, FRP reinforcement ratio, FRP elastic modulus...etc.).

The second part of the paper investigates the deformability capacity of FRP-RC beams to check whether certain limits in design should be defined to ensure that minimum deformability is provided by design for a full range of FRP-RC beams properties. This minimum deformability requirement is essential to ensure that FRP-RC beams will have sufficient deformability to show a warning before failure. The investigation is conducted by simulating a large number of beams with different specified properties and then evaluating their deformability behavior. To the authors' best knowledge, no explicit minimum deformability criterion was found in ACI 440 [7] or CSA S806 guidelines [45,46]; therefore, this study aims to establish such a criterion.

2. FRP-RC Database

2.1. Experimental dataset description

The experimental database used in this study consists of 164 test specimens of FRP-RC beams from experimental investigations carried out by several researchers [9-29]. The 164 tests covered three different reinforcing fiber materials: glass (GFRP), aramid (AFRP), and carbon (CFRP) material with different elastic modulus, tensile strength, and bar diameters. The differences in FRP bars material come down to differences in elastic modulus and tensile strength. The beams in the dataset also varied in their depth, width, FRP reinforcement ratio, and depth-to-width ratio. **Table 1** summarizes the range of the parameters in the dataset and **Fig. 2** shows the distribution of each parameter in the dataset. As observed in **Fig. 2**, ρ_f/ρ_b provides a good predictor of the failure mode (see the distribution of ρ_f/ρ_b). However, this does not mean that ρ_f/ρ_b alone is a robust predictor of the failure mode as this experimental database is of limited size; thus, the optimal decision boundary or the optimal predictors for classification cannot be fully defined. For example, in-depth assessment of **Fig. 2**, one would notice what looks like a linear decision boundary in ρ_f/ρ_b and b space or ρ_f/ρ_b and h space. Thus, to identify the optimal decision boundary or optimal predictors for classification, the database needs to be expanded. To do this, a verified analytical model is used to simulate more data to be used in the classification study.

This is a preprint draft. The published article can be found at: https://doi.org/10.1016/j.compstruct.2022.115651

Please cite this paper as:
Saleh E, Tarawneh, A., Naser M.Z., (2022). "Failure mode classification and deformability evaluation for concrete beams reinforced with FRP bars." *Composite Structures*. https://doi.org/10.1016/j.compstruct.2022.115651

126 **Table 1** Summary of the range of parameters in the collected dataset

f_{fu} MPa	E_f GPa	f_c' MPa	ρ_f/ρ_b		b mm	h mm	h/b
			FRP Rupture	Concrete crushing			
[513-2070]	[36-200]	[24-97]	[0.73-2]	[0.93-16.36]	[130-381]	[152-550]	[0.29-2.5]

f_{fu} = FRP tensile strength; E_f =FRP elastic modulus; f_c' = compressive strength of concrete; $\emptyset$ = dimeter of FRP bar; b = Beam width; h =Beam depth; $\rho_f = A_s/bd$ =FRP reinforcement ratio; d =beam effective depth; A_s = area of bottom FRP reinforcement; $\rho_b = 0.85\beta_1(f_c'/f_{fu})(E_f\ \varepsilon_{cu}/(E_f\ \varepsilon_{cu} + f_{fu}))$ = balanced reinforcement ratio; β_1 is a factor relating the compressive stress block to the neutral axis depth; ε_{cu} is the maximum concrete compressive stain (0.003 according to ACI 318).

127

This is a preprint draft. The published article can be found at: https://doi.org/10.1016/j.compstruct.2022.115651

Please cite this paper as:
Saleh E, Tarawneh, A., Naser M.Z., (2022). "Failure mode classification and deformability evaluation for concrete beams reinforced with FRP bars." *Composite Structures*. https://doi.org/10.1016/j.compstruct.2022.115651

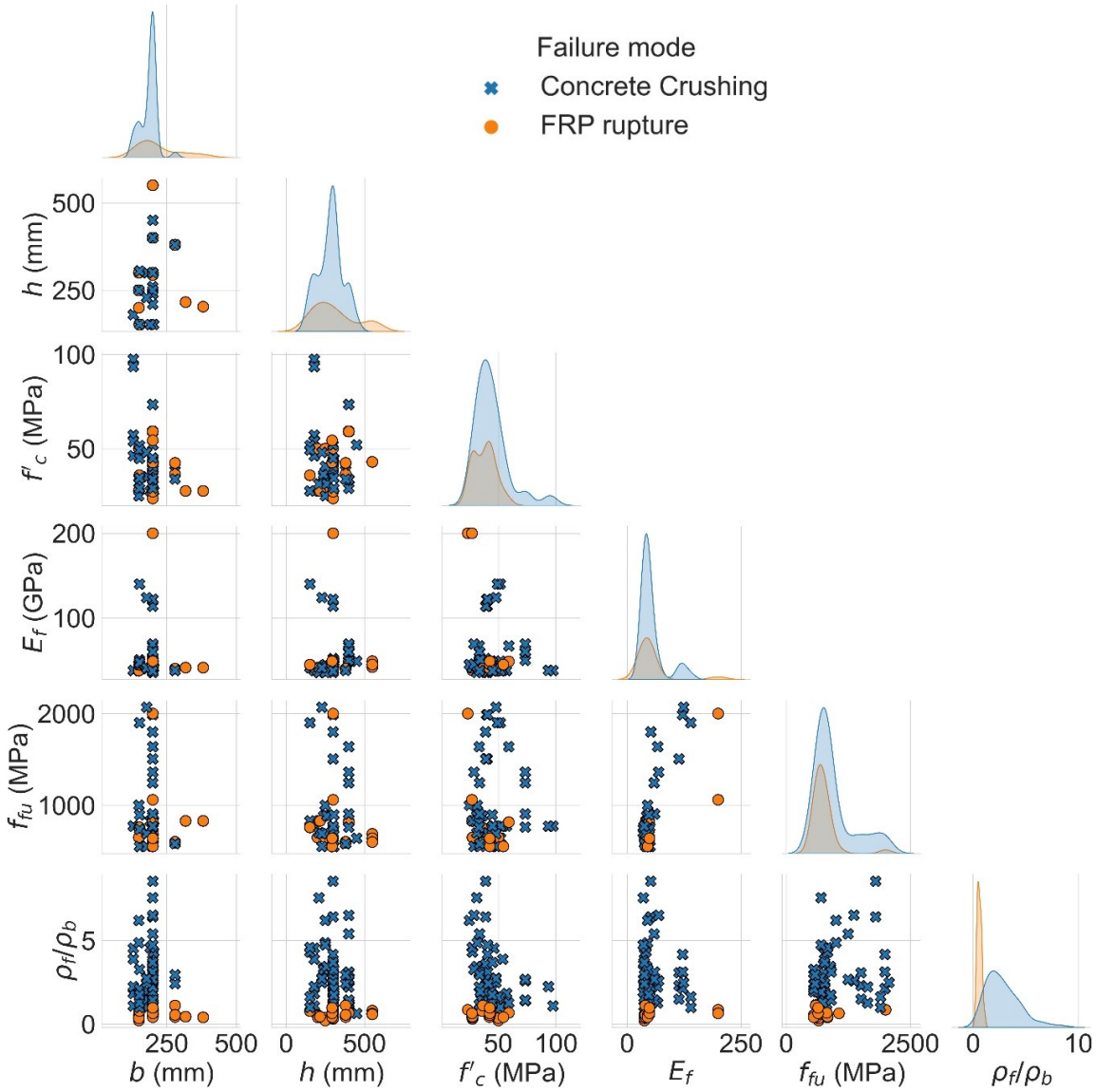

Fig. 2. Distribution of variables in the experimental database.

2.2. Analytical modeling and simulations

The Moment-curvature ($M - \Phi$) analysis is an accurate approach to determine the maximum flexural capacity of structural members that are primarily subjected to flexural failure mode using nonlinear stress-strain material relationships. The Moment-curvature diagrams can also be used to assess the ductility of structural members and the amount of plastic energy the member can absorb before failure.

This is a preprint draft. The published article can be found at: https://doi.org/10.1016/j.compstruct.2022.115651

Please cite this paper as:
Saleh E, Tarawneh, A., Naser M.Z., (2022). "Failure mode classification and deformability evaluation for concrete beams reinforced with FRP bars." *Composite Structures*. https://doi.org/10.1016/j.compstruct.2022.115651

For a certain axial load, there exists a strain value at the extreme compression fiber (ε_{cu}) that can be used to define a section curvature ($\Phi = \varepsilon_{cu}/c$; where c is the depth of the compression block) at which the applied axial load is in equilibrium with the nonlinear internal stress distribution. A certain moment capacity associated with this section curvature can be calculated from the stress distribution. The strain at the extreme compression fiber can be iterated until a range of $M - \Phi$ values is obtained. In our case, we are only interested in identifying the failure mode associated with certain geometric and material properties of FRP-RC beams. The $M - \Phi$ diagram can be used to identify this failure mode by tracing the values of the strain at the extreme compression fiber (ε_{cu}), and at the bottom layer of FRP reinforcement (ε_t). The strain value that reaches its limit before the other defines the failure mode. For example, if ε_t reaches the tensile strength limit before ε_{cu}, then the identified failure mode is FRP rupture.

A Fiber model is employed here to calculate the $M - \Phi$ curve of the FRP-RC beam as shown in **Fig. 3**. The concrete region of the beam was divided into rectangular layers (or patches). Each layer is assigned to a stress-stress relationship calculated using the Hongestad model [47] in compression and the tension-softening model [48] in tension. The FRP bars were assigned to a linear elastic stress-strain relationship until failure that occurs at an ultimate tensile strain of ε_{tu} or ultimate tensile stress of f_{fu}.

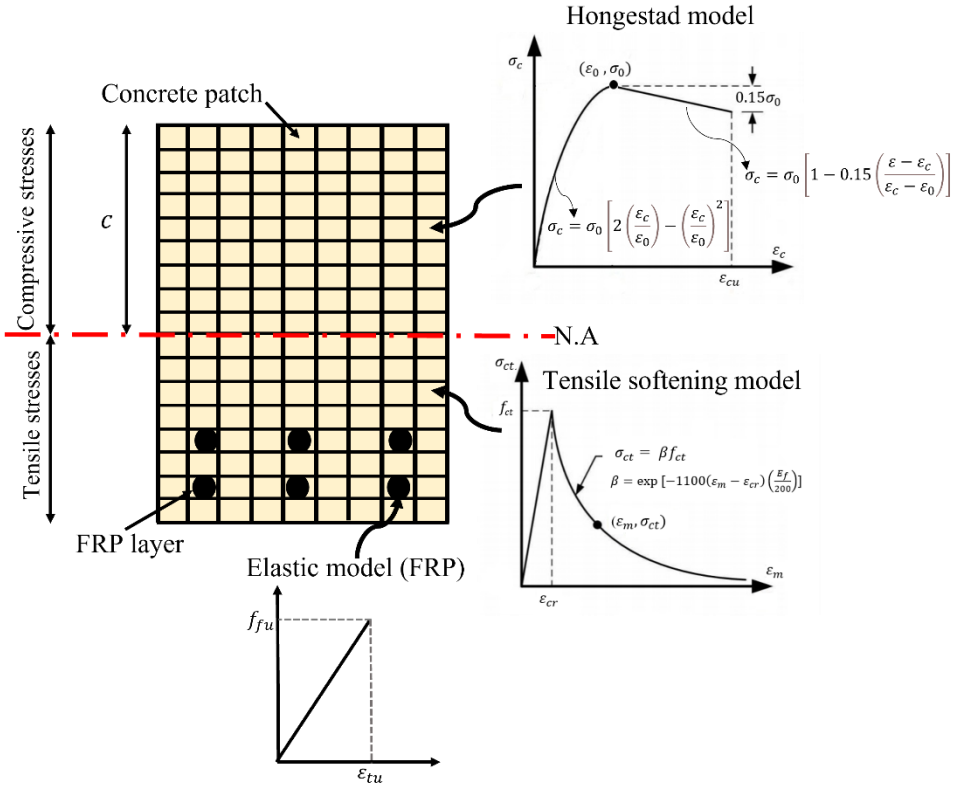

This is a preprint draft. The published article can be found at: https://doi.org/10.1016/j.compstruct.2022.115651

Please cite this paper as:
Saleh E, Tarawneh, A., Naser M.Z., (2022). "Failure mode classification and deformability evaluation for concrete beams reinforced with FRP bars." *Composite Structures*. https://doi.org/10.1016/j.compstruct.2022.115651

Fig. 3. The FRP-RC beam cross-section fiber model. The parameters of concrete models were determined based on the available data from [49].

The steps for calculating the $M-\Phi$ curve and identifying the failure mode using the fiber model are as follows:

- A value of the extreme compression fiber strain is assumed (starting with a small value).
- The compressive force at each patch in the compression region is estimated as the product of the area of the patch and the average stress that is determined based on the strain in the patch (assuming linear strain distribution, this strain can be determined using the extreme compression fiber strain) and the stress-strain relationship assumed for concrete in compression.
- The tensile force at each patch in the tensile region is estimated as the product of the area of the patch and the average stress that is determined based on the strain in the patch and the stress-strain relationship assumed for concrete in tension.
- The tensile force at the FRP layer is determined as the product of the area of FRP reinforcement and the FRP stress that is determined based on the strain value at the FRP location and the stress-strain relationship assumed for FRP in tension.
- The location of the neutral axis (c) is varied until equilibrium of the forces (zero) in the cross-section, for the assumed extreme compression fiber strain, is achieved.
- The moment is calculated by summing the moments of the forces about the neutral axis (N.A.).
- $M-\Phi$ curve is generated by iteratively increasing the extreme compression fiber strain and repeating the above steps to obtain a range of $M-\Phi$ values.
- If the extreme compression fiber strain reaches its ultimate value (ε_{cu}) before the FPR bars reach their tensile strain limit ($\varepsilon_{tu}=f_{fu}/E_f$), the beam is assigned to concrete crushing failure mode otherwise, it is assigned to the FRP rupture failure mode.

2.2.1. Validation of the analytical model

A correlation study between the experimental results and the analytical model shows the ability of the model to describe the behavior of the FRP-RC beam (see **Fig. 4** and **Table 1A** in the Appendix) with high accuracy. This correlation study results in an average experimental-to-predicted moment capacity M_{exp}/M_{pred} of 1.04 and a coefficient of variation of 0.07. In addition, the analytical model was able to predict the failure mode perfectly for all the experimental results (see **Table 1A**). Further, **Fig. 5** shows the ability of the analytical model to predict the moment-curvature relationship of the FRP reinforced beam by comparing predictions with experimental data.

This is a preprint draft. The published article can be found at: https://doi.org/10.1016/j.compstruct.2022.115651

Please cite this paper as:
Saleh E, Tarawneh, A., Naser M.Z., (2022). "Failure mode classification and deformability evaluation for concrete beams reinforced with FRP bars." *Composite Structures*. https://doi.org/10.1016/j.compstruct.2022.115651

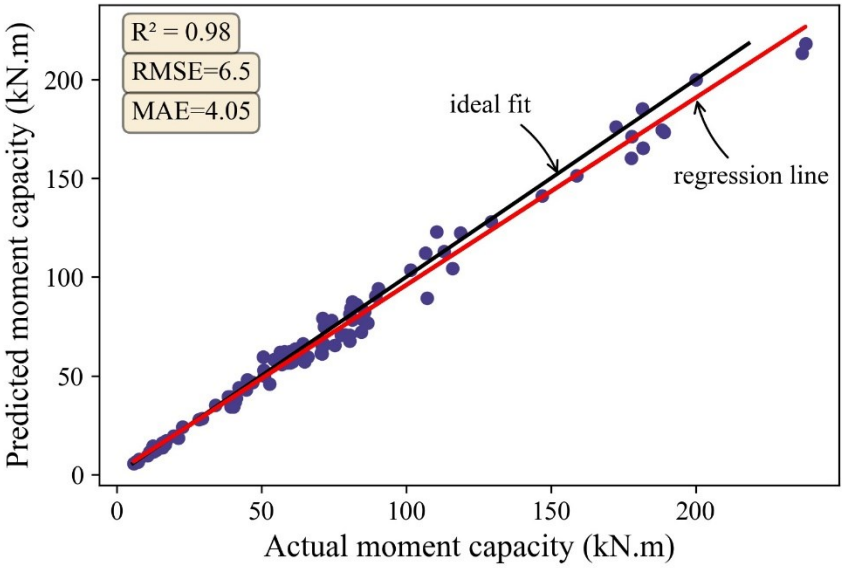

Fig. 4. Correlation curve between the predicted vs actual moment capacity of the beams in the dataset. (RMSE= root mean square error, MAE =maximum absolute error)

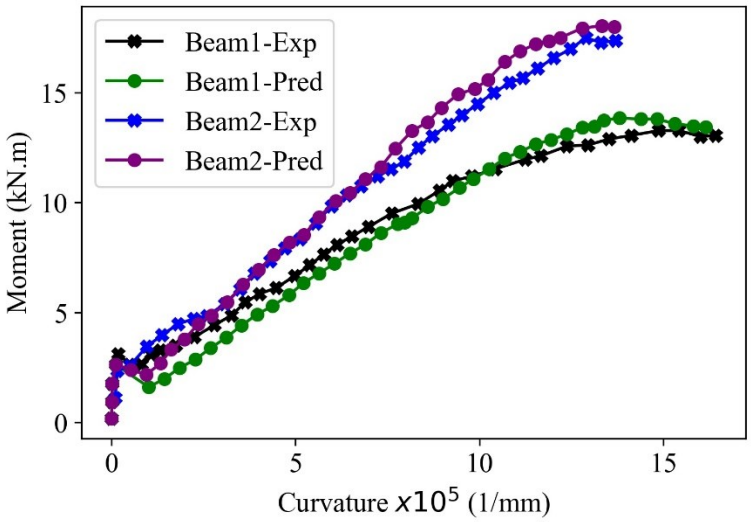

Fig. 5. Comparison between predicted (Pred) and experimental (Exp) moment-curvature relationship of FRP reinforced beam (Experimental data from [1])

2.2.3. Simulations using the developed analytical model.

Over 100,000 FRP-RC beams were simulated using the validated analytical model, each having a different combination of specified parameters that include: the longitudinal reinforcing FRP ratio ρ_f, the concrete cross-section dimension (b and h), the specified concrete strength f_c',

This is a preprint draft. The published article can be found at: https://doi.org/10.1016/j.compstruct.2022.115651

Please cite this paper as:
Saleh E, Tarawneh, A., Naser M.Z., (2022). "Failure mode classification and deformability evaluation for concrete beams reinforced with FRP bars." *Composite Structures*. https://doi.org/10.1016/j.compstruct.2022.115651

the stress at the FRP bars at failure f_{fu} and FRP modulus of elasticity E_f. The range of these parameters was selected considering the common and applicable ranges of these properties in the construction industry and the collected database.

Figure 6 shows the simulated data points and their associated mode of failure for different variables. From **Fig. 6**, it is apparent as before that ρ_f/ρ_b the ratio is a good classifier of the failure mode of FRP-RC beams, which can be seen by the separation between the density distributions associated with each failure mode concerning ρ_f/ρ_b. However, this will be checked against a robust classification method. In addition, even if ρ_f/ρ_b is enough as a classification parameter for the failure mode, investigating the cut-off value for classification and the optimal width of the margin of the transition zone is equally important. It should be noted that the discrepancy between simulated and experimental data is because the simulated data covers ranges of properties (material and cross-sectional properties) that experimental data does not cover.

This is a preprint draft. The published article can be found at: https://doi.org/10.1016/j.compstruct.2022.115651

Please cite this paper as:
Saleh E, Tarawneh, A., Naser M.Z., (2022). "Failure mode classification and deformability evaluation for concrete beams reinforced with FRP bars." *Composite Structures*. https://doi.org/10.1016/j.compstruct.2022.115651

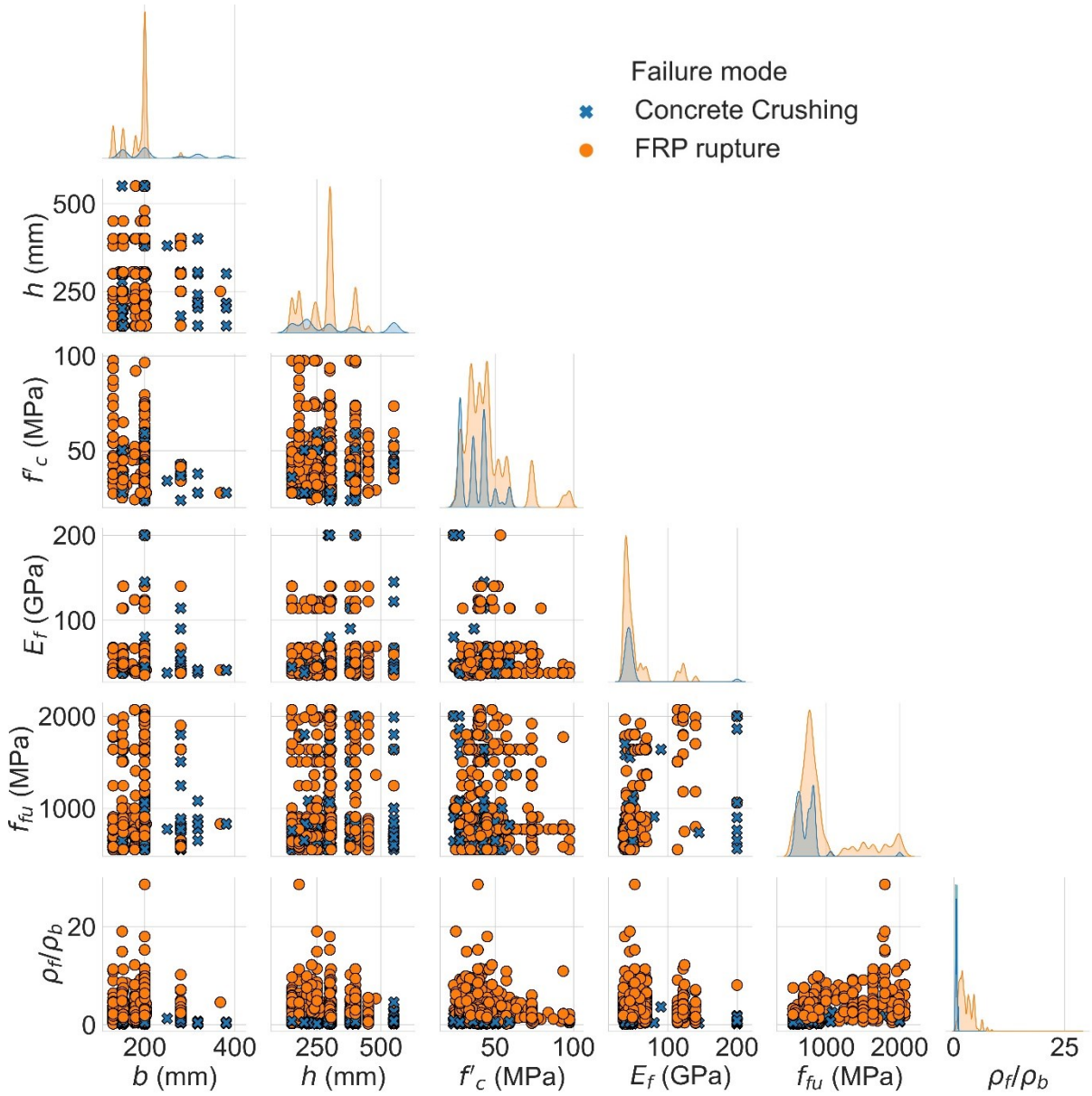

Fig. 6. The simulated FRP-RC beams and their associated mode of failure.

3. Classification study

In a classical classification problem, a training dataset consists of a set of features (predictor variables), and the response variable which is a categorical variable is utilized to learn a classification rule from the training dataset. After learning the classification rule, any new data point with a set of features can be classified and a class label will be assigned to it.

This is a preprint draft. The published article can be found at: https://doi.org/10.1016/j.compstruct.2022.115651

Please cite this paper as:
Saleh E, Tarawneh, A., Naser M.Z., (2022). "Failure mode classification and deformability evaluation for concrete beams reinforced with FRP bars." *Composite Structures*. https://doi.org/10.1016/j.compstruct.2022.115651

A support vector machine (SVM) has been a popular tool for classification tasks in the data modeling field [50]. SVM employs the principle of optimal separation hyperplane. This principle selects the hyperplane with the maximum margin as well as the one that minimizes the number of misclassifications errors [51]. When the data is linearly separable, SVM achieves an optimal classification rule. However, for non-linearly separable data, the kernel function can be utilized for transforming the data to a different dimension space where the data can be linearly separable [52]. SVM, given a training set, tries to construct a classifier of the form

$$y(x) = sign[\sum_{i=1}^{N} \alpha_i y_i k(x, x_i) + b] \quad \text{Eq. (1)}$$

Where α_i's and b are positive real constants; $k(x, x_i)$ is the kernel function, for linear SVM it takes the form $k(x, x_i) = x_i^T x$; x is the vector of predictors. Given an arbitrary training dataset, one cannot typically know the best kernel to be used in the classification. It is recommended to start the analysis by assuming the simplest hypothesis space (e.g., linear kernel) then working the way up toward the more complex kernels. If, for example, both RBF and linear kernels work equally well for a certain dataset, the simplest kernel is preferred (linear kernel) as it is less prone to overfitting. A comprehensive review of the literature on SVM and its applications in structural engineering can be found in [50,53].

In this study, the aim is to find an efficient and reliable classification rule for the failure mode of FRP-RC beams. The predictive variables represent the features that characterize FRP-RC beams which include: $E_f, f_{fu}, f_c', \rho_f/\rho_b$, and h/b. The training dataset used in the training of the SVM algorithm is from the simulated and experimental datasets discussed in the previous section.

3.1. Feature selection

Before classification, feature selection is preferred to be performed to remove all the trivial features that are not helpful in the classification [54]. In addition, it is desirable to reduce the number of features (or predictors) to make the model more interpretable and reduce its computational cost. Feature selection methods can be categorized, based on the mechanism of ranking and selecting the features, into three types: wrapper, filter, and embedded methods [54,55]. Here, the filter method will be employed for feature selection as it provides robustness against overfitting as opposed to the other feature selection methods [54,55]. Filter approaches, as the name implies, will first estimate the feature importance ranking and then use a filtering rule, such as a specified cut-off threshold, to remove all unnecessary features. The most common filter-based feature selection methods for numerical input features and categorical output (i.e., classification problems) are the mutual information statistics and ANOVA F-test [55]. Mutual information is a measure that quantifies the information gained for one variable given a known value of another variable while the ANOVA F-test measures the degree of the variability in one variable that can explain the variability in another variable. The process of using these methods for feature selection follow the below steps

- Calculate the mutual information or ANOVA measure between each input feature and the output feature (class label).

This is a preprint draft. The published article can be found at: https://doi.org/10.1016/j.compstruct.2022.115651

Please cite this paper as:
Saleh E, Tarawneh, A., Naser M.Z., (2022). "Failure mode classification and deformability evaluation for concrete beams reinforced with FRP bars." *Composite Structures*. https://doi.org/10.1016/j.compstruct.2022.115651

- Select the desired number of input features based on their mutual information or ANOVA measure (select the top-ranking features).
- Fit the model using the selected features.
- Test different numbers of input features to fit the model and discover the optimal number that results in the best performing model (tune the number of selected inputs).

As shown in **Fig. 7**, performing ANOVA and mutual information tests clearly show that ρ_f/ρ_b are the most relevant input feature to predict the failure mode. It can be also observed that E_f has a modestly low feature importance score, suggesting perhaps it can be removed. It should be noted that the feature h/b was selected instead of h or b because it is more practical to use at the beginning of the design process to check the failure mode.

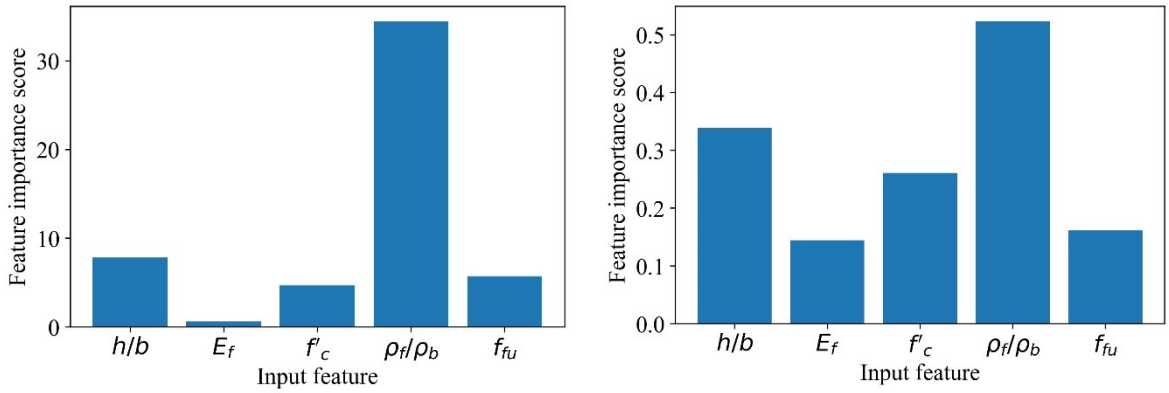

(a) ANOVA F-test (b)Mutual information

Fig. 7. Feature importance score of each input feature based on (a) ANOVA F-test (b) Mutual information measure.

Rather than guessing the best number of features, we can systematically perform a grid search to tune the number of selected features. This is done by evaluating the model (SVM classifier) using 10-fold cross-validation for different numbers of features. For tuning the number of selected features, a linear SVM classifier is considered (this choice will be verified later) while the performance of the models is measured using the average accuracy of 10-fold cross-validation. **Figure 8** shows the Box and whisker plots that are created for repeated 10-fold cross-validation results (i.e., for different splits of the data into training and testing sets). These Box and whisker plots show a trend of increasing mean average accuracy with the number of input features to two features (top two based on the importance score: ρ_f/ρ_b and h/b), after which the average accuracy becomes less stable. Thus, two features may be an appropriate choice for this classifier and dataset.

This is a preprint draft. The published article can be found at: https://doi.org/10.1016/j.compstruct.2022.115651

Please cite this paper as:
Saleh E, Tarawneh, A., Naser M.Z., (2022). "Failure mode classification and deformability evaluation for concrete beams reinforced with FRP bars." *Composite Structures*. https://doi.org/10.1016/j.compstruct.2022.115651

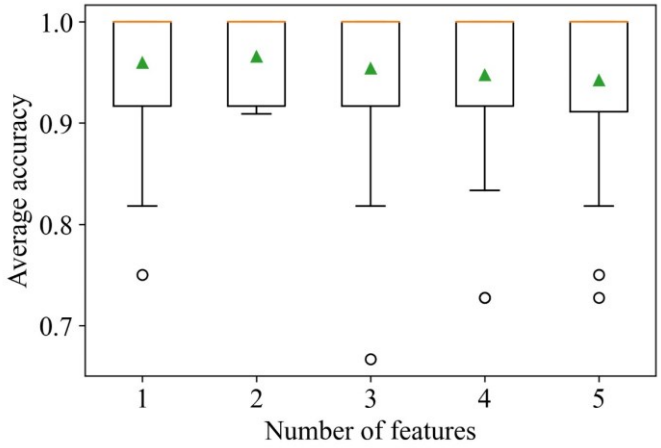

Fig. 8. Box and whisker plots show the relationship between the number of selected features and the average accuracy of the model. (Green markers represent the mean values).

To achieve the best performance SVM classifier, another parameter should be tuned is the kernel type [50]. **Table 2** shows that the linear kernel performed the best in classifying the failure mode with an average accuracy of 10-fold cross-validation of 97%; thus, will be employed here.

Table 2 Tuning of the SVM kernel

Kernel	Classification accuracy %
Linear	97%
Radial basis function (RBF)	95%
Polynomial	95.5%
Sigmoid	86%

3.2. Training the SVM classifier

The linear SVM classifier with a soft margin has only one parameter, a regularization parameter (C) that controls the width of the margin that separates the classes (i.e., failure modes). If C is small, a small penalty is added for the misclassified cases so a decision boundary will have a large margin while at large C, the classifier will try to minimize the number of misclassified cases which results in a decision boundary with a small margin. To choose an optimum C value that results in the best performing model, a 10-fold cross-validation procedure is performed as illustrated in **Fig. 9.** This procedure starts by splitting the data into a training set and testing set, then splitting the training set into 10 folds. Then the model is fitted using 9 folds and the remaining fold is used to validate the model (record the performance score of this fold). This process is repeated until every fold serves as the test set then the performance of the model is measured as the average performance of the test fold from all the iterations. This process is performed for different values of C to search for the optimal value (grid search). Once the optimal

This is a preprint draft. The published article can be found at: https://doi.org/10.1016/j.compstruct.2022.115651

Please cite this paper as:
Saleh E, Tarawneh, A., Naser M.Z., (2022). "Failure mode classification and deformability evaluation for concrete beams reinforced with FRP bars." *Composite Structures*. https://doi.org/10.1016/j.compstruct.2022.115651

hyperparameter (i.e., C) is obtained (i.e., C that results in the best performing model), the test set is used to assess the performance of the final model.

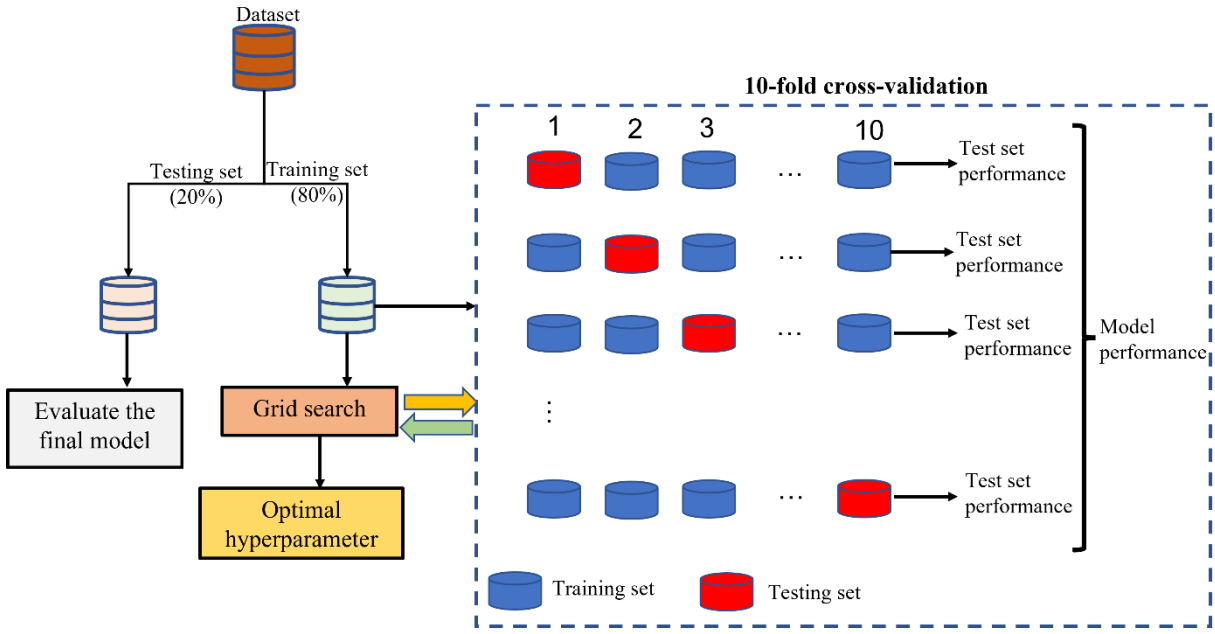

Fig. 9. Tuning of the hyperparameter

The final model obtained using the 10-fold cross-validation described above is illustrated in **Fig. 10.** From **Fig. 10**, it is obvious, that there is a dependence of the classification rule on the h/b ratio and ρ_f/ρ_b. Consequently, the failure mode of the FRP-RC beam can be classified as follows:

$$\text{Failure mode classification} \begin{cases} 3.85\ \rho_f/\rho_b - h/b - 3 \leq -1, & FRP\ rupture \\ -1 < 3.85\ \rho_f/\rho_b - h/b - 3 \leq 1 & Transition\ Zone \\ 3.85\ \rho_f/\rho_b - h/b - 3 \geq 1, & Concrete\ crushing \end{cases} \quad \text{Eq. (2)}$$

This is a preprint draft. The published article can be found at: https://doi.org/10.1016/j.compstruct.2022.115651

Please cite this paper as:
Saleh E, Tarawneh, A., Naser M.Z., (2022). "Failure mode classification and deformability evaluation for concrete beams reinforced with FRP bars." *Composite Structures*. https://doi.org/10.1016/j.compstruct.2022.115651

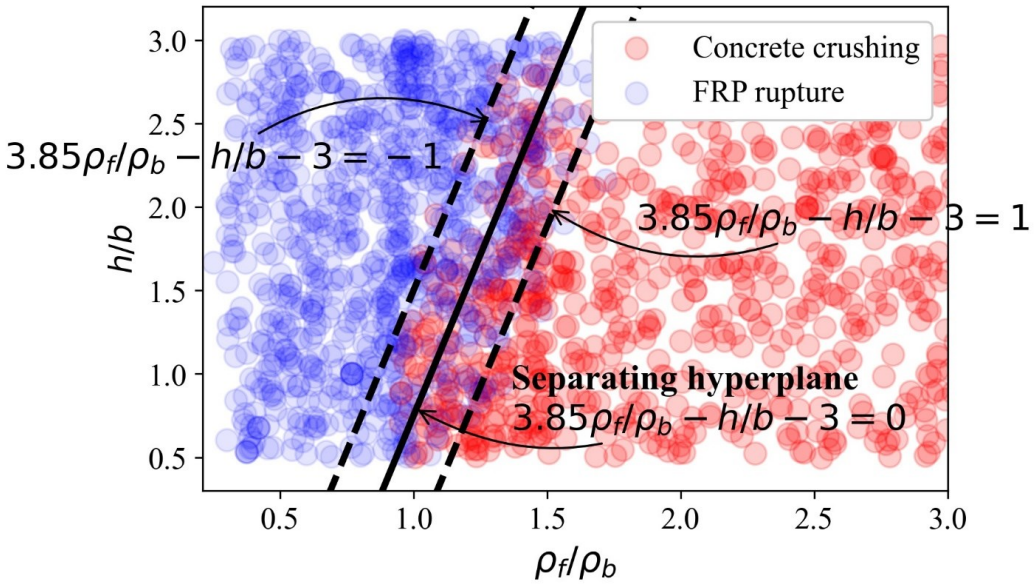

Fig. 10. Results of the classification using SVM. The figure also shows the hyperplane with a maximal margin of separation between the two different failure modes.

3.3. SVM performance

The performance of our SVM classifier cannot be directly evaluated as classical classifiers (e.g., based on the accuracy of the prediction) as the dataset only contains two failure modes while the data were classified, based on the developed SVM classifier, into three classes (i.e., concrete crushing, transition zone, and FRP rupture). To solve this, for performance evaluation, the data points inside the margin were excluded from the performance assessment.

The performance of the classifier is assessed based on the confusion matrix. The confusion matrix is a table that illustrates the actual failure modes versus the predicted failure modes by a certain classifier. The diagonal parts in the confusion matrix represent the number of correctly classified data points while the off-diagonal parts represent the number of incorrectly classified failure modes. For example, **Fig. 11a** shows the confusion matrix by the SVM classifier for the test set. The confusion matrix consists of two rows and two columns corresponding to the possible failure modes. The labels R and CC in the confusion matrix corresponds to the FRP rupture and concrete crushing failure mode, respectively. It is seen from **Fig. 11a** that 4782 FRP rupture failure modes and 14228 concrete crushing failure modes are predicted correctly by the SVM. The efficiency of the SVM classifier can be evaluated by the recall, precision, and accuracy of the confusion matrix. The recall is the percentile of correct prediction of a certain failure mode out of the actual data of this failure mode in the test set, and it is provided in the third row of the confusion matrix. Precision is the percentile of correct predictions for each failure mode, and it is shown in the third column of the confusion matrix. The total number of correct predictions of the failure

This is a preprint draft. The published article can be found at: https://doi.org/10.1016/j.compstruct.2022.115651

Please cite this paper as:
Saleh E, Tarawneh, A., Naser M.Z., (2022). "Failure mode classification and deformability evaluation for concrete beams reinforced with FRP bars." *Composite Structures*. https://doi.org/10.1016/j.compstruct.2022.115651

mode in the test set (i.e., the accuracy of the classifier) is shown at the last diagonal element in the confusion matrix. High recall, precision, and accuracy indicate the effectiveness of the classifier in identifying the correct failure mode. In **Fig. 11a,** the SVM classifier shows 95.8% and 97.8% precision in classifying the FRP rupture, and concrete crushing failure mode, respectively, and recalls of 93.6% and 98.6% in classifying the FRP rupture, and concrete crushing failure mode, respectively while the accuracy of the SVM classifier is 97%.

To compare the developed SVM classifier with existing classification rules, this study selects the ACI 440 classification method that is based only on ρ_f/ρ_b ratio (see **Fig. 1**). The classification results of this method for the test set are shown in **Fig. 11b** via the confusion matrix. It should be noted that the same test set is used to evaluate this rule and the SVM classifier. The overall accuracy of the ACI 440 classification rule is 87% with a precision of 94.7% for the FRP rupture failure mode. However, it shows a low recall of 64.3% for the FRP rupture failure mode, i.e., the ACI 440 method predicts only 4863 out of 7759 cases in the complete test set that exhibited FRP rupture failure mode as correct. A comparison of the SVM classifier and the ACI 440 clearly shows that the SVM classifier outperforms the ACI 440 classification rule in predicting the actual failure mode.

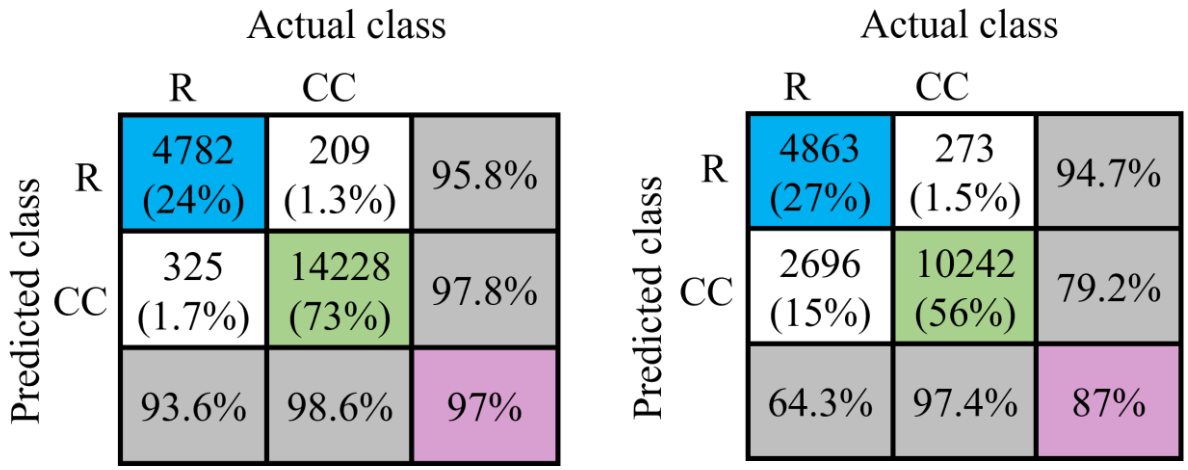

(a) The SVM classifier (b) ACI 440

Fig. 11. Performance evaluation of the (a) SVM classifier and (b) ACI 440 classification rule using the test set.

3.4. Sensitivity of the classification rule to random variations of parameters

At the beginning of the design, nominal values of parameters will be used in evaluating the strength capacity. However, these nominal values are subjected to random variations during construction due to several sources of uncertainty. To ensure that the specified reliability is

This is a preprint draft. The published article can be found at: https://doi.org/10.1016/j.compstruct.2022.115651

Please cite this paper as:
Saleh E, Tarawneh, A., Naser M.Z., (2022). "Failure mode classification and deformability evaluation for concrete beams reinforced with FRP bars." *Composite Structures*. https://doi.org/10.1016/j.compstruct.2022.115651

obtained in the design of FRP-RC beams, it is necessary to include possible variations in the design parameters when choosing the appropriate width of the transition region of classification, that characterizes by a greater factor of safety or smaller strength reduction factor than the concrete crushing region (see **Fig. 1**). Thus, we conducted a sensitivity analysis of the developed classification rule to random variations of design parameters. The sensitivity analysis process followed the flow chart depicted in **Fig. 12**.

In the sensitivity analysis, first, a range of nominal design parameters of the FRP-RC beams was selected then random variations to these parameters were included by multiplying the nominal value of each parameter by a random variable sampled from the associated distribution described in **Table 3**. These random variables represent the bias expected in the parameter value. Then, the actual failure mode from the analytical model was evaluated (true classification based on the actual properties of the FRP-RC beam). The SVM algorithm considering the nominal values of the features and actual prediction of the failure mode can then be used. Finally, the confidence interval of the margin width is estimated.

Table 3 Statistical properties of design parameters

Variable	Mean value	Coefficient of variation	Probability distribution	Reference
Cross section (b, h, d)	1.00	0.04	Normal	[56]
Concrete strength	$\lambda_{f'_c}$	0.10	Normal	[56]
Ultimate concrete compressive strain	1.00	0.15	Lognormal	[57]
FRP strength	1.18	0.12	Weibull	[8]
FRP modulus of elasticity in tension	1.04	0.08	Lognormal	[8]
Area of FRP	1.00	0.03	Normal	[8]

$\lambda_{f'_c} = -2.47 \times 10^{-5}(f'_c)^3 + 3.17 \times 10^{-3}(f'_c)^2 - 1.35 \times 10^{-1} f'_c + 3.0649 \geq 1.15 \quad (f'_c \text{ MPa})^*$

$\lambda_{f'_c}$: Bias in concrete compressive strength

This is a preprint draft. The published article can be found at: https://doi.org/10.1016/j.compstruct.2022.115651

Please cite this paper as:
Saleh E, Tarawneh, A., Naser M.Z., (2022). "Failure mode classification and deformability evaluation for concrete beams reinforced with FRP bars." *Composite Structures*. https://doi.org/10.1016/j.compstruct.2022.115651

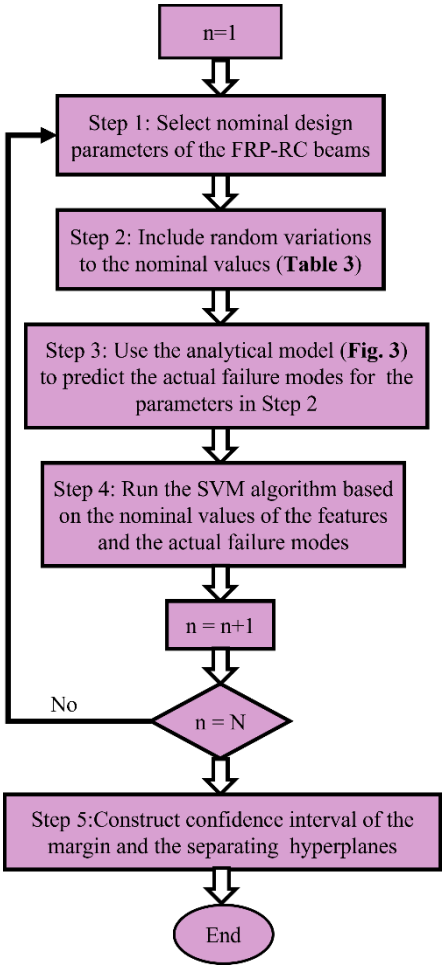

Fig. 12. Flow chart of the sensitivity analysis process. N= the predefined total number of simulations decided to construct the confidence interval.

From the sensitivity analysis, different classification rules for each simulation of beams (herein, step 1 consists of 10,000 beams for each simulation) were able to be defined. **Figure 13** shows the result of one of the simulations. It is evident from **Fig. 13** that randomness has an impact on the width of the margin, but the slope approximately remains unaffected by the original classification rule.

It should be noted that the experimental data points in **Fig. 13** were not used in the SVM algorithm since its features are assumed to belong to different probability distributions than what is listed in **Table 3** as they were constructed under high-quality control compared to the construction sites. It is depicted in the figure for demonstration purposes only.

This is a preprint draft. The published article can be found at: https://doi.org/10.1016/j.compstruct.2022.115651

Please cite this paper as:
Saleh E, Tarawneh, A., Naser M.Z., (2022). "Failure mode classification and deformability evaluation for concrete beams reinforced with FRP bars." *Composite Structures*. https://doi.org/10.1016/j.compstruct.2022.115651

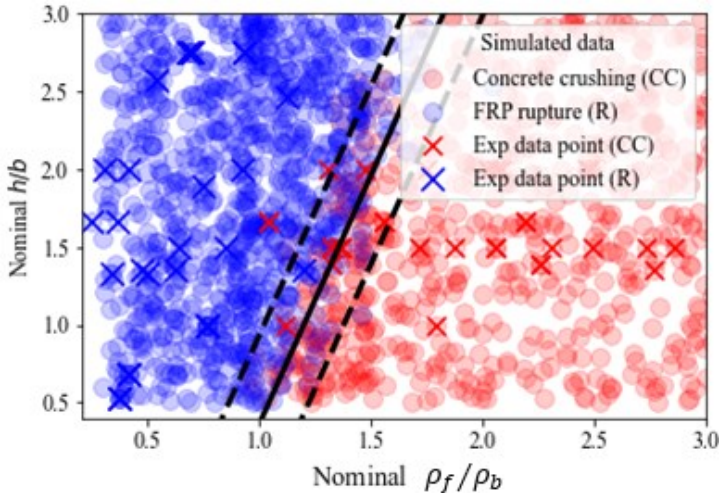

Fig. 13. Classification rule of one of the random simulations. Exp= Experimental

3.5. Final model

The results of the classification study are summarized in **Fig. 14**. The figure shows the proposed and ACI 440 classification intervals. Under the common h/b ratio of beams (i.e., most h/b of beams falls in the interval $[1.5-2]$) the margin does not deviate significantly from the defined margin in the ACI guideline. In addition, the classification rule was not affected significantly by the random variations of parameters. Based on the classification results, it is recommended to use the proposed classification equation or to shift the upper limit of the transition zone proposed by ACI 440 to be $1.55\rho_b$. A similar conclusion was reported in reference [8]. From **Fig. 14**, one could notice that this value corresponds to $h/b = 2$, within the common range of h/b for beams.

This is a preprint draft. The published article can be found at: https://doi.org/10.1016/j.compstruct.2022.115651

Please cite this paper as:
Saleh E, Tarawneh, A., Naser M.Z., (2022). "Failure mode classification and deformability evaluation for concrete beams reinforced with FRP bars." *Composite Structures*. https://doi.org/10.1016/j.compstruct.2022.115651

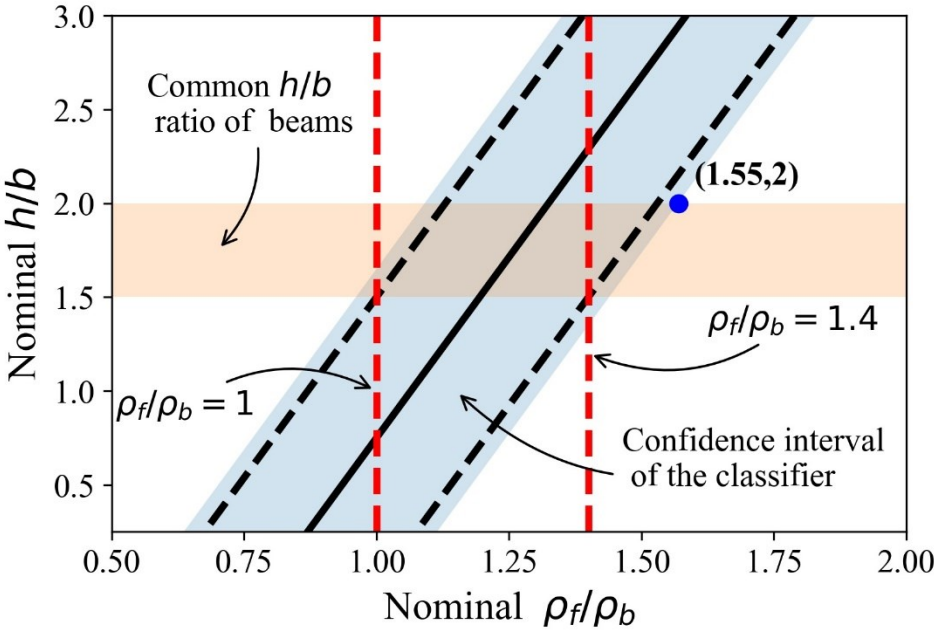

Fig. 14. Summary of the classification study results.

4. Deformability of FRP-RC flexural members

In steel reinforced concrete members, the determination of deformability is based on the strain in steel tension reinforcement at the ultimate stage [58]. A higher strain in steel reinforcement is associated with increased curvature and deflection which yields more warning to the public [8, 59]. ACI 318-19 classify members with a reinforcement strain of at least 0.005 as tension-controlled sections, and a higher resistance factor is specified. Assuming a concrete strain ε_{cu} of 0.003 at the ultimate stage and a reinforcement strain limit ε_t of 0.005 as commonly accepted by ACI, the curvature limit Φ can be determined by dividing the sum of strains by the depth to the extreme layer of reinforcement d,

$$\Phi = \frac{\varepsilon_{cu}+\varepsilon_t}{d} = \frac{0.008}{d} \quad \text{Eq. (3)}$$

Therefore, if $\Phi \times d \geq 0.008$, the strain limit of reinforcement will meet the criteria of tension-controlled members [8]. According to Gulbrandsen 2005 [59], the values of $\Phi \times d$ at the ultimate of FRP-RC beams exceeds 0.008 for both modes of failure (tensile rupture and concrete crushing) which is the limit at which steel reinforcement concrete members are deemed as tension-controlled members. However, this conclusion was based on the analysis of a small number of beams (20 beams) and did not consider a wide range of parameters. This study is providing a comprehensive evaluation of the deformability behavior of FRP-RC beams to ensure that minimum deformability is implicitly provided by the design, and if an additional restriction on the FRP reinforcement strain

This is a preprint draft. The published article can be found at: https://doi.org/10.1016/j.compstruct.2022.115651

Please cite this paper as:
Saleh E, Tarawneh, A., Naser M.Z., (2022). "Failure mode classification and deformability evaluation for concrete beams reinforced with FRP bars." *Composite Structures*. https://doi.org/10.1016/j.compstruct.2022.115651

or reinforcement ratio is required, similar to ACI 318 strain requirement for steel-RC members (i.e., Based on ACI 318-19 code, flexural must be tension controlled $\varepsilon_s \geq 0.005$).

To evaluate the deformability of FRP-RC beams, a reference for comparison purposes needs to be set, herein a tension-controlled limit for steel-RC members is chosen. To define the maximum steel reinforcement ratio necessary to reach a tension-controlled state, the stress and strain distribution of a typical reinforced concrete member is considered. **Figure 15** shows the common representation of stresses and strains for a typical reinforced concrete beam. Where c represents the neutral axis depth; A_s representing the area of reinforcement; d is the distance from the top of the section to the centroid of the reinforcement (effective depth); d_t is the distance from the top of the section to the extreme layer of reinforcement, and f_s is the stress in the tension reinforcement.

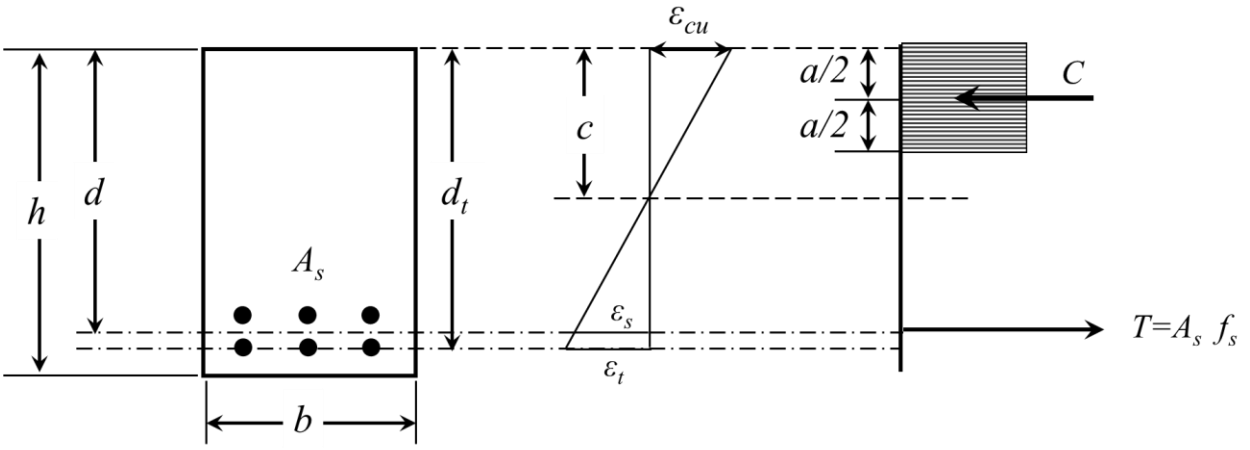

Fig. 15. Stress and strain distribution of a typical reinforced concrete section.

From **Fig. 15** the following relation can be obtained:

$$\frac{c}{d_t} = \frac{\varepsilon_{cu}}{\varepsilon_{cu}+\varepsilon_t} \quad \text{Eq. (4)}$$

and the depth of the compression block a: can be obtained using equilibrium

$$a = \frac{A_s\ f_y}{0.85 f_c' b} \quad \text{Eq. (5)}$$

Recalling that $a = \beta_1 c$ and the steel reinforcement ratio is defined as $\rho_s = \frac{A_s}{bd}$. Using Eq. (4) and (5), the reinforcement ratio can be obtained as follows:

$$\rho_s = \frac{0.85\beta_1 f_c' b}{f_s} \frac{\varepsilon_{cu}}{\varepsilon_{cu}+\varepsilon_t} \left(\frac{d}{d_t}\right) \quad \text{Eq. (6)}$$

This is a preprint draft. The published article can be found at: https://doi.org/10.1016/j.compstruct.2022.115651

Please cite this paper as:
Saleh E, Tarawneh, A., Naser M.Z., (2022). "Failure mode classification and deformability evaluation for concrete beams reinforced with FRP bars." *Composite Structures*. https://doi.org/10.1016/j.compstruct.2022.115651

Now, substituting $\varepsilon_{cu} = 0.003$, $\varepsilon_t = 0.005$, $f_s = f_y$, and assuming one layer of reinforcement (i.e., $d = d_t$) in Eq. (13), one obtains the maximum level to obtain tension-controlled failure in the steel-reinforced concrete section ρ_{TCL} [58]:

$$\rho_{TCL} = \frac{2.55\beta_1 f_c'}{8 f_y} \quad \text{Eq. (7)}$$

Following, more than 10,000 FRP-RC beams were simulated using the verified analytical model. Each beam has a different combination of specified parameters that include: the longitudinal reinforcing FRP ratio ρ_f, the concrete cross-section dimension (b and h), the specified concrete strength f_c', the stress at the FRP bars at failure f_{fu} and FRP modulus of elasticity E_f. The selection was based on the common ranges of these properties in the construction industry. The ranges of these parameters are shown in **Table 4**. The deformability of the simulated beams was determined using the relation $\Phi \times d$ (curvature × effective depth), resulting from the analysis of these FRP-RC beams specified in **Table 4** and the steel-reinforced concrete beams specified in **Table 5**. The Code limitation on strain for steel-reinforced concrete beams was based on the yield strain of grade 60 ksi (G420 MPa) steel. Thus, FRP-RC beams deformability were only compared to steel reinforced concrete beams with a grade 60 steel, where the baseline for comparison was the limit of deformability of tension-controlled steel reinforced concrete members was set (i.e., $\rho_s = \rho_{TCL}$).

Table 4 Specified properties of FRP-RC beams studied.

Parameter	Specified range	Number of specified values
f_{fu} MPa (psi)	300, 500, 700, 800, 1000, 1200	6
$E_f{}^*$ GPa	45; 80; 150**	3
f_c' MPa (psi)	24; 27.6; 34.5; 41.4; 55.2 (3000; 4000; 5000; 6000; 8000)	5
ρ/ρ_b	0.8; 0.9; 1;1.1;1.2;1.3;1.4,1.5;2;3;4;5	12
h mm	180 ; 300; 550	3
h/b	1.5, 1.75, 2	3

The total number of simulated beams is about 10,000 with each beam having a different combination of specified properties.
* High E_f is usually correlated with high f_{fu}
** 45, 80, and 150 GPa corresponds to GFRP, AFRP, and CFRP, respectively.

Table 5 Specified properties of steel-reinforced concrete beams that are used as a reference.

Parameter	Specified range	Number of specified values
f_y	Gr. 60 steel, $f_y = 420\ Mpa\ (60\ ksi)$	1
E_s	200 GPa (29000 ksi)	1

This is a preprint draft. The published article can be found at: https://doi.org/10.1016/j.compstruct.2022.115651

Please cite this paper as:
Saleh E, Tarawneh, A., Naser M.Z., (2022). "Failure mode classification and deformability evaluation for concrete beams reinforced with FRP bars." *Composite Structures*. https://doi.org/10.1016/j.compstruct.2022.115651

f_c' MPa (psi)	24; 27.6;34.5;41.4;55.2 (3000;4000;5000;6000;8000)	5
ρ_{TCL}	$2.55\beta_1 f_c'/8f_y$	--
h mm	180; 300;550	3
h/b	1.5,1.75,2	3

The total number of simulated steel-reinforced concrete beams equals ($1\times 1\times 5\times 3\times 3 = 45$) with each beam having a different combination of specified properties.

4.1. Results of the Deformability Analysis

The results of the deformability analysis are summarized in **Fig. 16** and **17**. As can be seen in **Fig. 16**, FRP-RC beams exhibit deformability values that are closely similar for both failure modes: concrete crushing and FRP rupture. In addition, results showed that FRP-RC beams that failed in concrete crushing mode exhibit a marginally larger variability in $\Phi \times d$ (curvature × effective depth) values. This leads to the conclusion that the FRP reinforcement ratio has an insignificant impact on the deformability of FRP-RC beams. The significant contributing factors to the deformability of FRP-RC beams, identified from conducted sensitivity analysis, are: E_f and f_{fu} , and their interaction. **Figure 17** shows deformability levels across these two variables*:* E_f and f_{fu}. Thus, to ensure minimum deformability requirements, a limit should be specified on (E_f/f_{fu}) ratio (the larger this factor the smaller the deformability expected in the member) rather than a limit on the FRP reinforcement ratio as the case in steel-reinforced beams (i.e., $\rho \leq \rho_{max}$).

Based on the analysis, it is proposed to limit the ratio (E_f/f_{fu}) to 200 to ensure sufficient deformability of FRP-RC beams (i.e., $E_f/f_{fu} \leq 200$) that need to be checked within the design process. Comparing FRP-RC beams to tension-controlled steel reinforced concrete members (**Fig. 16**), $\Phi \times d$ resulted in FRP-RC beams are higher deformability than what is required by the ACI code to classify as tension-controlled members indicating that FRP-RC beams will have sufficient deformability to show a warning before failure. Finally, from **Fig. 16** it is noted that beams with higher elastic modulus $\Phi \times d$ seem to exhibit lower variability.

This is a preprint draft. The published article can be found at: https://doi.org/10.1016/j.compstruct.2022.115651

Please cite this paper as:
Saleh E, Tarawneh, A., Naser M.Z., (2022). "Failure mode classification and deformability evaluation for concrete beams reinforced with FRP bars." *Composite Structures*. https://doi.org/10.1016/j.compstruct.2022.115651

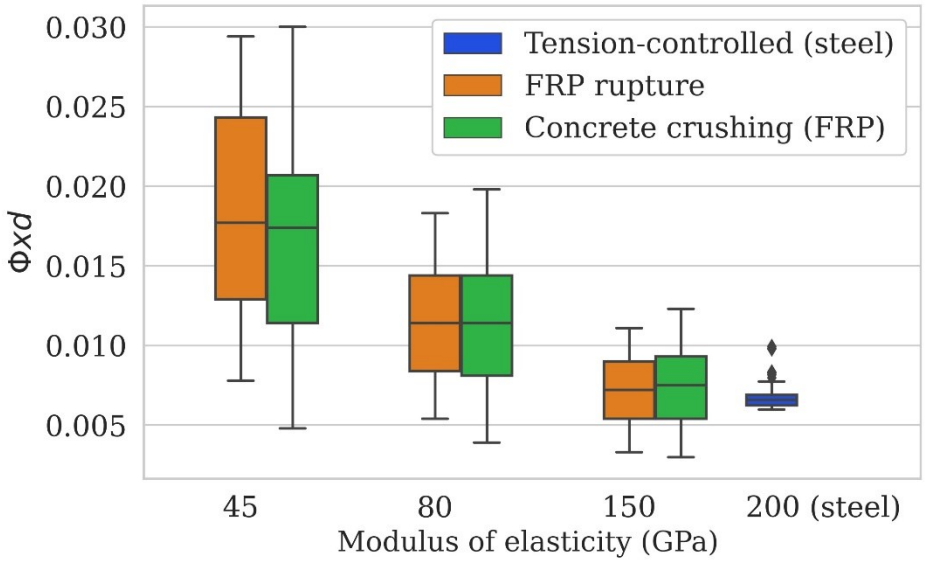

Fig. 16. Deformability levels are represented by Φ × d at different modulus of elasticity and failure modes.

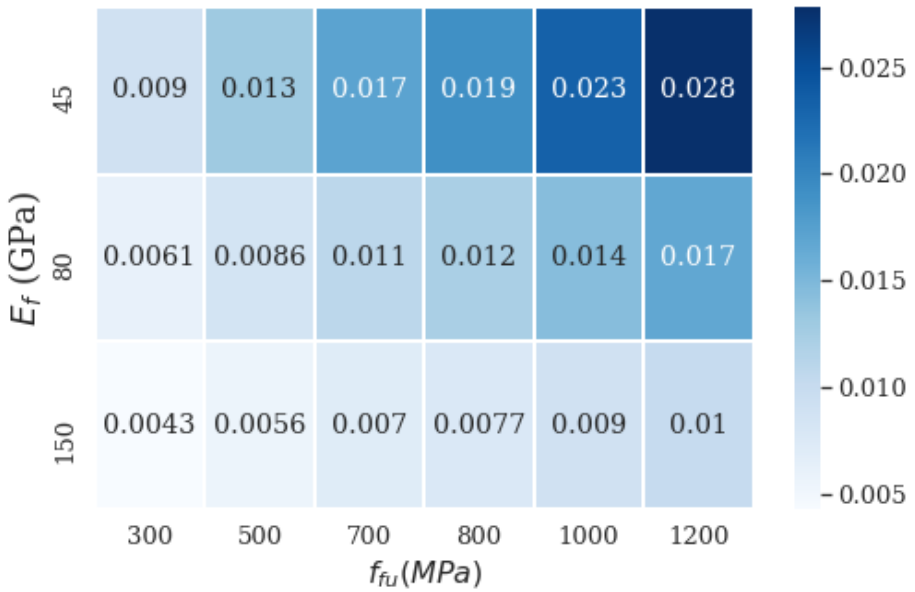

Fig. 17. Heat map displaying the average deformability levels represented by Φ × d across the two-axis variables: E_f and f_{fu}.

5. Conclusions

This is a preprint draft. The published article can be found at: https://doi.org/10.1016/j.compstruct.2022.115651

Please cite this paper as:
Saleh E, Tarawneh, A., Naser M.Z., (2022). "Failure mode classification and deformability evaluation for concrete beams reinforced with FRP bars." *Composite Structures*. https://doi.org/10.1016/j.compstruct.2022.115651

This paper presents the SVM technique to classify the failure mode of FRP-RC beams. To train the algorithm, first, 164 tests of FRP-RC beams tested for flexure failure were collected then used to verify an analytical model based on a sectional analysis of the FRP-RC section. The verified analytical model was used to simulate more than 100,000 FRP-RC beams data for classification development. The simulated beams combined with actual data of tested FRP-RC beams were used in the classification study. The study also provides a comprehensive deformability evaluation for FRP-RC beams. According to the results, the following conclusions can be drawn:

- The SVM algorithm demonstrates good accuracy for the classification of the failure mode of FRP-RC beams. The accuracy for the failure mode classification is 97% while the ACI guideline specification has an accuracy of 87%.
- Feature selection method identified ρ_f/ρ_b and h/b as the highest importance features among the available features for predicting the failure mode of FRP-RC beams. The following classification criterion is proposed

$$\text{Failure mode classification} \begin{cases} 3.85\ \rho_f/\rho_b - h/b - 3 \leq -1, & FRP\ rupture \\ -1 < 3.85\ \rho_f/\rho_b - h/b - 3 \leq 1 & Transition\ Zone \\ 3.85\ \rho_f/\rho_b - h/b - 3 \geq 1, & Concrete\ crushing \end{cases}$$

- Under the common h/b ratio of beams (i.e., most h/b of beams falls in the interval $[1.5-2]$) the margin does not deviate a lot from the defined margin in the ACI guideline. However, it is recommended to increase the upper limit for the transition zone to 1.55 compared to 1.4 specified in ACI 440.1R or to use the proposed classification criteria.
- The classification rule, learned using the SVM algorithm, was not affected significantly by the random variations of parameters.
- FRP-RC beams exhibit deformability values that are closely similar for both failure modes: concrete crushing and FRP rupture failure.
- Comparing FRP-RC beams to tension-controlled steel reinforced concrete members the available deformability resulted in FRP-RC beams are mostly larger than what is required by the ACI 318 guidelines to classify as tension-controlled members indicating that FRP-RC beams will have sufficient deformability to show a warning before failure.
- FRP reinforcement ratio has an insignificant impact on the deformability of FRP-RC beams. The top contributing factors to the deformability of FRP-RC beams, identified from conducted sensitivity analysis, are: E_f and f_{fu} , and their interaction.
- To ensure minimum deformability requirements for FRP-RC beams, a limit should be specified on (E_f/f_{fu}) ratio. Based on the analysis, a proposed limit of 200 (i.e., $E_f/f_{fu} \leq 200$) to ensure that a minimum (curvature) ×(effective depth) is greater than 0.008 which is the limit that classifies steel-reinforced concrete members as tension-controlled members.

Data availability

Row data are available upon request to the authors.

This is a preprint draft. The published article can be found at: https://doi.org/10.1016/j.compstruct.2022.115651

Please cite this paper as:
Saleh E, Tarawneh, A., Naser M.Z., (2022). "Failure mode classification and deformability evaluation for concrete beams reinforced with FRP bars." *Composite Structures*. https://doi.org/10.1016/j.compstruct.2022.115651

References

[1] Kara, Ilker Fatih, and Ashraf F. Ashour. "Flexural performance of FRP reinforced concrete beams." *Composite structures* 94, no. 5 (2012): 1616-1625.

[2] Al-Sunna, Raed, Kypros Pilakoutas, Iman Hajirasouliha, and Maurizio Guadagnini. "Deflection behaviour of FRP reinforced concrete beams and slabs: An experimental investigation." *Composites Part B: Engineering* 43, no. 5 (2012): 2125-2134.

[3] Ju, Minkwan, Younghwan Park, and Cheolwoo Park. "Cracking control comparison in the specifications of serviceability in cracking for FRP reinforced concrete beams." *Composite Structures* 182 (2017): 674-684.

[4] De Luca, A.; Matta, F.; and Nanni, A., "Behavior of Full-Scale Glass Fiber-Reinforced Polymer Reinforced Concrete Columns under Axial Load," *ACI Structural Journal*, V. 107, No. 5, Sept.-Oct. 2010, pp. 589-596.

[5] Wight, J.K., 2016. Reinforced concrete mechanics and design 7th edition. Pearson Education, Inc., Hoboken, New Jersey 07030.

[6] Peng, F. and Xue, W., 2019. Reliability Analysis of Eccentrically Loaded Concrete Rectangular Columns Reinforced with Fiber-Reinforced Polymer Bars. ACI Structural Journal, 116(4), pp.275-284.

[7] ACI Committee 440, 2015, "Guide for the Design and Construction of Structural Concrete Reinforced with FRP Bars (ACI 440.1R-15)," American Concrete Institute, Farmington Hills, MI, 83 pp.

[8] Shield, Carol K., Theodore V. Galambos, and Peter Gulbrandsen. "On the history and reliability of the flexural strength of FRP reinforced concrete members in ACI 440.1 R." *Special Publication* 275 (2011): 1-18.

[9] Benmokrane, B. and Masmoudi, R., 1996. Flexural response of concrete beams reinforced with FRP reinforcing bars. Structural Journal, 93(1), pp.46-55.

[10] AlMusallam TH, Al-Salloum YA, Alsayed SH, Amjad MA. Behavior of concrete beams doubly reinforced by FRP bars. In: Proceedings of the third international symposium on non-metallic (FRP) reinforcement for concrete structures (FRPRCS-3), Japan, vol. 2; 1997. p. 471–478.

[11] The´riault M, Benmokrane B. Effects of FRP reinforcement ratio and concrete strength on flexural behavior of concrete beams. J Compos Constr 1998;2(1):7–16.

[12] Toutanji HA, Saafi M. Flexural behavior of concrete beams reinforced with glass fiber-reinforced polymer (GFRP) bars. ACI Struct J 2000;97(5):712–9.

[13] Kassem C, Farghaly AS, Benmokrane B. Evaluation of flexural behavior and serviceability performance of concrete beams reinforced with FRP Bars. J Compos Constr 2011; doi:10.1061/(ASCE)CC.1943-5614.0000216 .

[14] Benmokrane B, Chaallal O, Masmoudi R. Glass fibre reinforced plastic (GFRP) rebars for concrete structures. Constr Build Mater 1995;9(6):353–364.

This is a preprint draft. The published article can be found at: https://doi.org/10.1016/j.compstruct.2022.115651

Please cite this paper as:
Saleh E, Tarawneh, A., Naser M.Z., (2022). "Failure mode classification and deformability evaluation for concrete beams reinforced with FRP bars." *Composite Structures*. https://doi.org/10.1016/j.compstruct.2022.115651

[15] Ashour AF. Flexural and shear capacities of concrete beams reinforced with GFPR bars. Constr Build Mater 2006; 20:1005–15.
[16] Benmokrane B, Chaallal O, Masmoudi R. Flexural response of concrete beams reinforced with FRP reinforcing bars. ACI Struct J 1996;91(2):46–55.
[17] Yost JR, Goodspeed CH, Schmeckpeper ER. Flexural performance of concrete beams reinforced with FRP grids. J Compos Constr 2001;5(1):18–25.
[18] Masmoudi R, The´riault M, Benmokrane B. Flexural behavior of concrete beams reinforced with deformed fiber reinforced plastic reinforcing rods. ACI Struct J 1998;95(6):665–76.
[19] Brown VL, Bartholomew CL. FRP reinforcing bars in reinforced concrete members. ACI Mater J 1993;90(1):34–9.
[20] Duranovic N, Pilakoutas K, Waldron P. Tests on concrete beams reinforced with galss fibre reinforced plastic bars. In: Proceedings of the third international symposium on non-metallic (FRP) reinforcement for concrete structures (FRPRCS 3), Japan, vol. 2; 1997. p. 479–86.
[21] Alsayed SH, Al-Salloum YA, Almusallam TH. Performance of glass fiber reinforced plastic bars as a reinforcing material for concrete structures. Compos Part 2000; 31: 555-567.
[22] Ashour AF, Habeeb MN. Continuous concrete beams reinforced with CFRP bars, StructBuild 2008; SB6: 349-357.
[23] Thiagarajan G. Experimental and analytical behavior of carbon fiber-based rods as flexural reinforcement. J Compos Constr, 2003; 7(1): 64-72.
[24] El-Nemr A, Ahmed EA, Benmokrane B. Flexural behavior and serviceability of normal-and high-strength concrete beams reinforced with glass fiber-reinforced polymer bars. ACI Struct J 2013;110(6):1077–87. https://doi.org/10.14359/ 51686162.
[25] Faza SS. Bending and bond behavior and design of concrete beams reinforced with fiber-reinforced plastic rebars. West Virginia University Libraries; 1991.
[26] by H. Wang, A. Belarbi, and B. Huanzi Wang, "Flexural Behavior of Fiber- Reinforced-Concrete Beams Reinforced with FRP Rebars," Oct. 2005. doi: 10.14359/14872.
[27] Lau D, Pam HJ. Experimental study of hybrid FRP reinforced concrete beams. Eng Struct 2010;32(12):3857–65. https://doi.org/10.1016/j.engstruct.2010.08.028.
[28] D. Gao and B. Benmokrane, "Calculation method of flexural capacity of GFRP-reinforced concrete beam," ASCE J. Hydraul. Eng., pp. 73–80, 2001.
[29] Japan Society of Civil Engineers, 1997. Recommendation for design and construction of concrete structures using continuous fiber reinforcing materials. Concrete engineering Series No.23, 325 pp.
[30] Alwanas, A.A.H., Al-Musawi, A.A., Salih, S.Q., Tao, H., Ali, M. and Yaseen, Z.M., 2019. Load-carrying capacity and mode failure simulation of beam-column joint connection: Application of self-tuning machine learning model. *Engineering Structures*, *194*, pp.220-229.
[31] Naser, M.Z., 2020. Machine learning assessment of fiber-reinforced polymer-strengthened and reinforced concrete Members. *ACI Structural Journal*, *117*(6), pp.237-251.

This is a preprint draft. The published article can be found at: https://doi.org/10.1016/j.compstruct.2022.115651

Please cite this paper as:
Saleh E, Tarawneh, A., Naser M.Z., (2022). "Failure mode classification and deformability evaluation for concrete beams reinforced with FRP bars." *Composite Structures*. https://doi.org/10.1016/j.compstruct.2022.115651

[32] Almustafa, M.K. and Nehdi, M.L., 2021. Machine learning prediction of structural response for FRP retrofitted RC slabs subjected to blast loading. *Engineering Structures*, *244*, p.112752.
[33] Huang, H. and Burton, H.V., 2019. Classification of in-plane failure modes for reinforced concrete frames with infills using machine learning. *Journal of Building Engineering*, *25*, p.100767.
[34] Naderpour, H., Mirrashid, M. and Parsa, P., 2021. Failure mode prediction of reinforced concrete columns using machine learning methods. *Engineering Structures*, *248*, p.113263.
[35] Mangalathu, S. and Jeon, J.S., 2019. Machine learning–based failure mode recognition of circular reinforced concrete bridge columns: Comparative study. *Journal of Structural Engineering*, *145*(10), p.04019104.
[36] Mangalathu, S., Hwang, S.H. and Jeon, J.S., 2020. Failure mode and effects analysis of RC members based on machine-learning-based SHapley Additive exPlanations (SHAP) approach. *Engineering Structures*, *219*, p.110927.
[37] Feng, D.C., Liu, Z.T., Wang, X.D., Jiang, Z.M. and Liang, S.X., 2020. Failure mode classification and bearing capacity prediction for reinforced concrete columns based on ensemble machine learning algorithm. *Advanced Engineering Informatics*, *45*, p.101126.
[38] Su, M., Zhong, Q., Peng, H. and Li, S., 2021. Selected machine learning approaches for predicting the interfacial bond strength between FRPs and concrete. *Construction and Building Materials*, *270*, p.121456.
[39] Kiani, J., Camp, C. and Pezeshk, S., 2019. On the application of machine learning techniques to derive seismic fragility curves. *Computers & Structures*, *218*, pp.108-122.
[40] Wang, Z., Pedroni, N., Zentner, I. and Zio, E., 2018. Seismic fragility analysis with artificial neural networks: Application to nuclear power plant equipment. *Engineering Structures*, *162*, pp.213-225.
[41] Naser, M.Z. and Salehi, H., 2020. Machine learning-driven assessment of fire-induced concrete spalling of columns. *ACI Mater J*, *117*(6), pp.7-16.
[42] Naser, M.Z., 2019. Heuristic machine cognition to predict fire-induced spalling and fire resistance of concrete structures. *Automation in Construction*, *106*, p.102916.
[43] Naser, M.Z. and Kodur, V.K., 2022. Explainable machine learning using real, synthetic and augmented fire tests to predict fire resistance and spalling of RC columns. *Engineering Structures*, *253*, p.113824.
[44] Feng, D.C., Cetiner, B., Azadi Kakavand, M.R. and Taciroglu, E., 2021. Data-driven approach to predict the plastic hinge length of reinforced concrete columns and its application. *Journal of Structural Engineering*, *147*(2), p.04020332.
[45] CSA (Canadian Standards Association). (2010). "Specification for fibre reinforced polymers." CAN/CSAS807, Rexdale, ON, Canada.
[46] CSA (Canadian Standards Association). (2012). "Design and construction of building structures with fibre-reinforced polymers." CAN/CSA S806-12, Rexdale, ON, Canada
[47] Hongestad, E., N. W. Hanson, and D. Mchenry. "Concrete stress distribution in ultimate design." In *ACI Journal, Proceedings*, vol. 52, no. 6, pp. 455-479. 1955.

This is a preprint draft. The published article can be found at: https://doi.org/10.1016/j.compstruct.2022.115651

Please cite this paper as:
Saleh E, Tarawneh, A., Naser M.Z., (2022). "Failure mode classification and deformability evaluation for concrete beams reinforced with FRP bars." *Composite Structures*. https://doi.org/10.1016/j.compstruct.2022.115651

[48] Bischoff, Peter H., and Richard Paixao. "Tension stiffening and cracking of concrete reinforced with glass fiber reinforced polymer (GFRP) bars." *Canadian Journal of Civil Engineering* 31, no. 4 (2004): 579-588.
[49] Qin, R., Zhou, A. and Lau, D., 2017. Effect of reinforcement ratio on the flexural performance of hybrid FRP reinforced concrete beams. *Composites Part B: Engineering*, *108*, pp.200-209.
[50] Noble, William S. "What is a support vector machine?." *Nature biotechnology* 24, no. 12 (2006): 1565-1567.
[51] Suthaharan, Shan. "Support vector machine." In *Machine learning models and algorithms for big data classification*, pp. 207-235. Springer, Boston, MA, 2016.
[52] Widodo, Achmad, and Bo-Suk Yang. "Support vector machine in machine condition monitoring and fault diagnosis." *Mechanical systems and signal processing* 21, no. 6 (2007): 2560-2574.
[53] Çevik, Abdulkadir, Ahmet Emin Kurtoğlu, Mahmut Bilgehan, Mehmet Eren Gülşan, and Hasan M. Albegmprli. "Support vector machines in structural engineering: a review." *Journal of Civil Engineering and Management* 21, no. 3 (2015): 261-281.
[54] Dash, Manoranjan, and Huan Liu. "Feature selection for classification." *Intelligent data analysis* 1, no. 1-4 (1997): 131-156.
[55] Wah, Yap Bee, Nurain Ibrahim, Hamzah Abdul Hamid, Shuzlina Abdul-Rahman, and Simon Fong. "Feature Selection Methods: Case of Filter and Wrapper Approaches for Maximising Classification Accuracy." *Pertanika Journal of Science & Technology* 26, no. 1 (2018).
[56] Nowak, A. S., & Szerszen, M. M. (2003). Calibration of design code for buildings (ACI 318): Part 1-Statistical models for resistance. *ACI Structural Journal*, *100*(3), 377-382.
[57] Baji, H., and Ronagh, H. R., 2016, "Reliability-Based Study on Ductility Measures of Reinforced Concrete Beams in ACI 318," ACI Structural Journal, V. 113, No. 2, Mar.-Apr., pp. 373-382. doi: 10.14359/51688201
[58] Orozco, Carlos E. "Strain limits vs. reinforcement ratio limits–A collection of new and old formulas for the design of reinforced concrete sections." *Case Studies in Structural Engineering* 4 (2015): 1-13.
[59] Gulbrandsen, Peter West. "Reliability Analysis of the Flexural Capacity of Fiber Reinforced Polymer Bars in Concrete Beams." PhD diss., University of Minnesota, 2005.

This is a preprint draft. The published article can be found at: https://doi.org/10.1016/j.compstruct.2022.115651

Please cite this paper as:
Saleh E, Tarawneh, A., Naser M.Z., (2022). "Failure mode classification and deformability evaluation for concrete beams reinforced with FRP bars." *Composite Structures*. https://doi.org/10.1016/j.compstruct.2022.115651

643 **APPENDIX A1**

644 **Table 1A** Collected experimental database. The last column shows the validation of the failure
645 mode predicted by the analytical model

Reference	Beam notation	Width (mm)	Overall depth (mm)	fc' MPa	A_s bottom (mm^2)	E (Gpa)	f_{ult} MPa	M_{exp} kN.m	Experimental mode of failure	M_{exp}/M_{pred} kN.m	Predicted failure mode
[7]	COMP-00	200	240	35.3	508.06	43.37	885	41.37	Concrete Crushing	1.07	Concrete Crushing
	COMP-25	200	240	35.3	508.06	43.37	885	39.06	Concrete Crushing	1.01	Concrete Crushing
	COMP-50	200	240	36.4	508.06	43.37	885	39.35	Concrete Crushing	1.00	Concrete Crushing
	COMP-75	200	240	36.4	508.06	43.37	885	40.6	Concrete Crushing	1.03	Concrete Crushing
[8]	BC2HA	130	180	57.2	237.65	38	773	19.7	Concrete Crushing	1.01	Concrete Crushing
	BC2HB	130	180	57.2	237.65	38	773	20.6	Concrete Crushing	1.05	Concrete Crushing
	BC2VA	130	180	97.4	237.65	38	773	22.7	Concrete Crushing	0.94	Concrete Crushing
	BC4NB	130	180	46.2	475.29	38	773	20.6	Concrete Crushing	1.07	Concrete Crushing
	BC4HA	130	180	53.9	475.29	38	773	21	Concrete Crushing	1.09	Concrete Crushing
	BC4HB	130	180	53.9	475.29	38	773	21.4	Concrete Crushing	1.16	Concrete Crushing
	BC4VA	130	180	93.5	475.29	38	773	28.4	Concrete Crushing	1.02	Concrete Crushing
	BC4VB	130	180	93.5	475.29	38	773	29.5	Concrete Crushing	1.04	Concrete Crushing
[9]	GB1-1	180	300	35	253.35	40	695	60	Concrete Crushing	1.06	Concrete Crushing
	GB1-2	180	300	35	253.35	40	695	59	Concrete Crushing	1.04	Concrete Crushing
	GB2-1	180	300	35	380.03	40	695	65	Concrete Crushing	1.14	Concrete Crushing
	GB2-2	180	300	35	380.03	40	695	64.3	Concrete Crushing	0.97	Concrete Crushing
	GB3-1	180	300	35	506.71	40	695	71	Concrete Crushing	1.16	Concrete Crushing
	GB3-2	180	300	35	506.71	40	695	70.5	Concrete Crushing	1.15	Concrete Crushing
[10]	C1-4	200	300	40.4	283.528	114	1506	71.2	Concrete Crushing	0.90	Concrete Crushing
	C1-6	200	300	39.3	425.29	114	1506	83.13	Concrete Crushing	0.97	Concrete Crushing
	C1-8	200	300	39.3	567.05	114	1506	90.39	Concrete Crushing	0.96	Concrete Crushing
	C2-4	200	300	39.9	254.46	122	1988	78.75	Concrete Crushing	1.11	Concrete Crushing
	C2-6	200	300	40.8	381.703	122	1988	80.89	Concrete Crushing	0.96	Concrete Crushing
	C2-8	200	300	40.8	508.93	122	1988	89.39	Concrete Crushing	0.99	Concrete Crushing
	G1-6	200	300	39.05	760.06	40	617	77.47	Concrete Crushing	1.10	Concrete Crushing
	G1-8	200	300	39.05	1013.4	40	617	86.76	Concrete Crushing	1.13	Concrete Crushing

This is a preprint draft. The published article can be found at: https://doi.org/10.1016/j.compstruct.2022.115651

Please cite this paper as:
Saleh E, Tarawneh, A., Naser M.Z., (2022). "Failure mode classification and deformability evaluation for concrete beams reinforced with FRP bars." *Composite Structures*. https://doi.org/10.1016/j.compstruct.2022.115651

	G2-6	200	300	39.05	678.58	36	747	71	Concrete Crushing	1.09	Concrete Crushing
	G2-8	200	300	39.05	904.77	36	747	84.54	Concrete Crushing	1.17	Concrete Crushing
	AR-6	200	300	39.05	425.29	52	1800	70.85	Concrete Crushing	1.05	Concrete Crushing
	AR-8	200	300	39.05	567.05	52	1800	71.75	Concrete Crushing	0.96	Concrete Crushing
[11]	ISO30-2	200	300	44	573.04	42	689	80.4	Concrete Crushing	0.99	Concrete Crushing
	KD30-1	200	300	44	573.04	49	641	50.6	Concrete Crushing	0.85	Concrete Crushing
	KD30-2	200	300	44	573.04	49	641	63.8	Concrete Crushing	1.08	Concrete Crushing
	KD45-1	200	450	52	573.04	49	641	106.6	Concrete Crushing	0.95	Concrete Crushing
	KD45-2	200	450	52	573.04	49	641	113	Concrete Crushing	1.00	Concrete Crushing
	ISO55-1	200	550	43	573.04	42	689	181.5	FRP rupture	0.98	FRP rupture
	ISO55-2	200	550	43	573.04	42	689	181.5	FRP rupture	0.98	FRP rupture
	KD55-1	200	550	43	573.04	49	641	146.9	FRP rupture	1.04	FRP rupture
	KD55-2	200	550	43	573.04	49	641	172.5	FRP rupture	0.98	FRP rupture
[12]	Beam2	150	200	50.09	113.10	38	650	16.75	FRP rupture	1.10	FRP rupture
	Beam4	150	250	27.68	56.55	38	650	5.886	FRP rupture	1.04	FRP rupture
	Beam6	150	300	27.68	56.55	38	650	7.848	FRP rupture	1.00	FRP rupture
	beam8	150	200	27.68	56.55	38	650	10.791	FRP rupture	1.13	FRP rupture
	beam10	150	250	50.09	56.55	38	650	5.886	FRP rupture	1.04	FRP rupture
	beam12	150	300	50.09	113.10	38	650	16.75	FRP rupture	1.10	FRP rupture
[13]	ISO2	200	300	43	573.04	45	600	80.4	Concrete Crushing	1.14	Concrete Crushing
	ISO3	200	550	43	573.04	45	600	181.7	FRP rupture	1.10	FRP rupture
	ISO4	200	550	43	573.04	45	600	181.7	FRP rupture	1.10	FRP rupture
[14]	1FRP1	381	203	27.6	80.00	41.4	830	11.49	FRP rupture	1.00	FRP rupture
	1FRP2	381	203	27.6	80.00	41.4	830	12.67	FRP rupture	1.11	FRP rupture
	1FRP3	381	203	27.6	80.00	41.4	830	11.49	FRP rupture	1.00	FRP rupture
	2FRP1	318	216	27.6	80.00	41.4	830	13.62	FRP rupture	1.11	FRP rupture
	2FRP2	318	216	27.6	80.00	41.4	830	13.26	FRP rupture	1.08	FRP rupture
	2FRP3	318	216	27.6	80.00	41.4	830	13.06	FRP rupture	1.06	FRP rupture
	4FRP1	203	152	27.6	320.00	41.4	830	15.78	Concrete Crushing	1.16	Concrete Crushing
	4FRP2	203	152	27.6	320.00	41.4	830	15.58	Concrete Crushing	0.98	Concrete Crushing

This is a preprint draft. The published article can be found at: https://doi.org/10.1016/j.compstruct.2022.115651

Please cite this paper as:
Saleh E, Tarawneh, A., Naser M.Z., (2022). "Failure mode classification and deformability evaluation for concrete beams reinforced with FRP bars." *Composite Structures*. https://doi.org/10.1016/j.compstruct.2022.115651

	4FRP3	203	152	27.6	320.00	41.4	830	16.29	Concrete Crushing	1.02	Concrete Crushing
	5FRP1	191	152	27.6	320.00	41.4	830	16.37	Concrete Crushing	1.03	Concrete Crushing
	5FRP2	191	152	27.6	320.00	41.4	830	16.65	Concrete Crushing	1.05	Concrete Crushing
	5FRP3	191	152	27.6	320.00	41.4	830	15.78	Concrete Crushing	0.99	Concrete Crushing
[15]	CB2B-1	200	300	52	348.73	37.6	773	57.9	Concrete Crushing	0.93	Concrete Crushing
	CB2B-2	200	300	52	348.73	37.6	773	59.8	Concrete Crushing	0.96	Concrete Crushing
	CB3B-1	200	300	52	523.10	37.6	773	66	Concrete Crushing	1.11	Concrete Crushing
	CB3B-2	200	300	52	523.10	37.6	773	64.8	Concrete Crushing	1.08	Concrete Crushing
	CB4B-1	200	300	45	697.46	37.6	773	75.4	Concrete Crushing	1.15	Concrete Crushing
	CB4B-2	200	300	45	697.46	37.6	773	71.7	Concrete Crushing	1.09	Concrete Crushing
	CB6B-1	200	300	45	1046.20	37.6	773	84.8	Concrete Crushing	1.08	Concrete Crushing
	CB6B-2	200	300	45	1046.20	37.6	773	85.4	Concrete Crushing	1.09	Concrete Crushing
[16]	1	152	152	35.9	70.88218	44.8	760	7.04	FRP rupture	1.09	FRP rupture
	2	152	152	35.9	70.88218	44.8	760	6.64	FRP rupture	1.03	FRP rupture
	4	152	152	35.9	70.88218	44.8	760	7.23	FRP rupture	1.12	FRP rupture
	5	152	152	35.9	70.88218	44.8	760	7.35	FRP rupture	1.13	FRP rupture
	6	152	152	35.9	70.88	44.8	760	6.75	FRP rupture	1.05	FRP rupture
[17]	GB5	150	250	24.96	429.42	45	1000	40.3	Concrete Crushing	1.17	Concrete Crushing
	GB9	150	250	31.84	429.42	45	1000	39.73	Concrete Crushing	1.15	Concrete Crushing
	GB10	150	250	31.84	429.42	45	1000	39.5	Concrete Crushing	1.15	Concrete Crushing
[18]	II	200	210	31.3	1134.11	35.63	700	34.1875	Concrete Crushing	0.97	Concrete Crushing
	III	200	260	31.3	506.71	43.37	886	45.125	Concrete Crushing	0.94	Concrete Crushing
	IV	200	300	40.7	567.06	35.63	700	59.1875	Concrete Crushing	0.99	Concrete Crushing
	V	200	250	40.7	1134.11	35.63	700	57	Concrete Crushing	1.02	Concrete Crushing
[19]	C-C-3[a]	200	300	23.6	88.36	200	2000	44.76	FRP rupture	1.04	FRP rupture
	C-C-4[a]	200	300	27.2	226.19	200	1061	60.66	FRP rupture	1.06	FRP rupture
[20]	B4	152.4	152.4	51.73	63.34	140	1900	12.603	Concrete Crushing	0.87	Concrete Crushing
	B7	152.4	152.4	49.3	99.03	140	1900	17.104	Concrete Crushing	1.00	Concrete Crushing
[21]	N2#13G2	200	400	33.5	261.17	67	1639	82.78	Concrete Crushing	0.96	Concrete Crushing
	N3#13G1	200	400	33.5	384.89	48.7	817	81.34	Concrete Crushing	0.93	Concrete Crushing

This is a preprint draft. The published article can be found at: https://doi.org/10.1016/j.compstruct.2022.115651

Please cite this paper as:
Saleh E, Tarawneh, A., Naser M.Z., (2022). "Failure mode classification and deformability evaluation for concrete beams reinforced with FRP bars." *Composite Structures*. https://doi.org/10.1016/j.compstruct.2022.115651

	H2#13G2	200	400	59.1	261.17	67	1639	101.59	Concrete Crushing	0.98	Concrete Crushing
	H3#13G1	200	400	59.1	384.89	48.7	817	85.58	FRP rupture	1.04	FRP rupture
	N5#15G2	200	400	29	970.37	69.3	1362	129.32	Concrete Crushing	1.01	Concrete Crushing
	N6#15G1	200	400	33.5	1161.89	50	762	118.73	Concrete Crushing	0.97	Concrete Crushing
	H5#15G2	200	400	73.4	970.37	69.3	1362	178	Concrete Crushing	1.04	Concrete Crushing
	H6#15G1	200	400	73.4	1161.89	50	762	177.73	Concrete Crushing	1.11	Concrete Crushing
	N5#15G3	200	400	33.8	970.37	59.5	1245	110.58	Concrete Crushing	0.90	Concrete Crushing
	N2#25G3	200	400	33.8	1019.25	60.3	906	115.93	Concrete Crushing	1.11	Concrete Crushing
	H5#15G3	200	400	73.4	1039.98	59.5	1245	188.37	Concrete Crushing	1.08	Concrete Crushing
	H2#25G3	200	400	73.4	1019.25	60.3	906	189.06	Concrete Crushing	1.09	Concrete Crushing
[22]	C4	152.4	304.8	28.95799	1012.90	45.5	551.5808	54.24	Concrete Crushing	0.93	Concrete Crushing
	C8	152.4	304.8	34.4738	774.19	50.6	551.5808	56.45028	Concrete Crushing	0.91	Concrete Crushing
	C-H5	152.4	304.8	44.81594	1006.45	45.5	551.5808	74.241	Concrete Crushing	0.95	Concrete Crushing
	CC	152.4	304.8	44.81594	1006.45	45.5	551.5808	81.36	Concrete Crushing	1.04	Concrete Crushing
	EH2	152.4	304.8	44.81594	380.64	48.3	737.73932	42.21228	Concrete Crushing	0.96	Concrete Crushing
	EH4	152.4	304.8	44.81594	354.84	47.7	896.3188	50.85	Concrete Crushing	0.96	Concrete Crushing
[23]	P4G	178	229	48	219.00	124	2069	51	Concrete Crushing	1.00	Concrete Crushing
	P8G	178	229	48	723.00	41	690	47	Concrete Crushing	1.01	Concrete Crushing
	P4C	178	229	48	1077.00	41	552	51	Concrete Crushing	1.02	Concrete Crushing
[24]	G0.8-A90	280	380	36.6	804.20	40	593	158.8	FRP rupture	1.05	FRP rupture
	G2.1-A90	280	380	41.3	1963.50	38	582	237.93	Concrete Crushing	1.09	Concrete Crushing
	G0.4-A135	280	380	42.3	339.30	40.2	603	80.4	FRP rupture	1.19	FRP rupture
	G0.5-A135	280	380	42.5	452.40	40.2	603	107.3	FRP rupture	1.20	FRP rupture
	G2.1-A135	280	380	33.9	1963.50	38	582	236.78	Concrete Crushing	1.11	Concrete Crushing
[25]	IS2B-1	200	293.5	42.66667	299.13	45	552	38.5	FRP rupture	0.98	FRP rupture
	IS2B-2	200	293.5	54.4	299.13	45	552	41	FRP rupture	1.12	FRP rupture
	KD2B-1	200	293.5	42.66667	299.13	49	641	52.8	FRP rupture	1.15	FRP rupture
	KD2B-2	200	293.5	42.66667	449.20	49	641	61.6	FRP rupture	0.97	FRP rupture
	CB6B-2	200	300	45	1046.20	37.6	773	85.4	Concrete Crushing	1.09	Concrete Crushing

646